A holistic time-series analysis of stony coral tissue loss disease

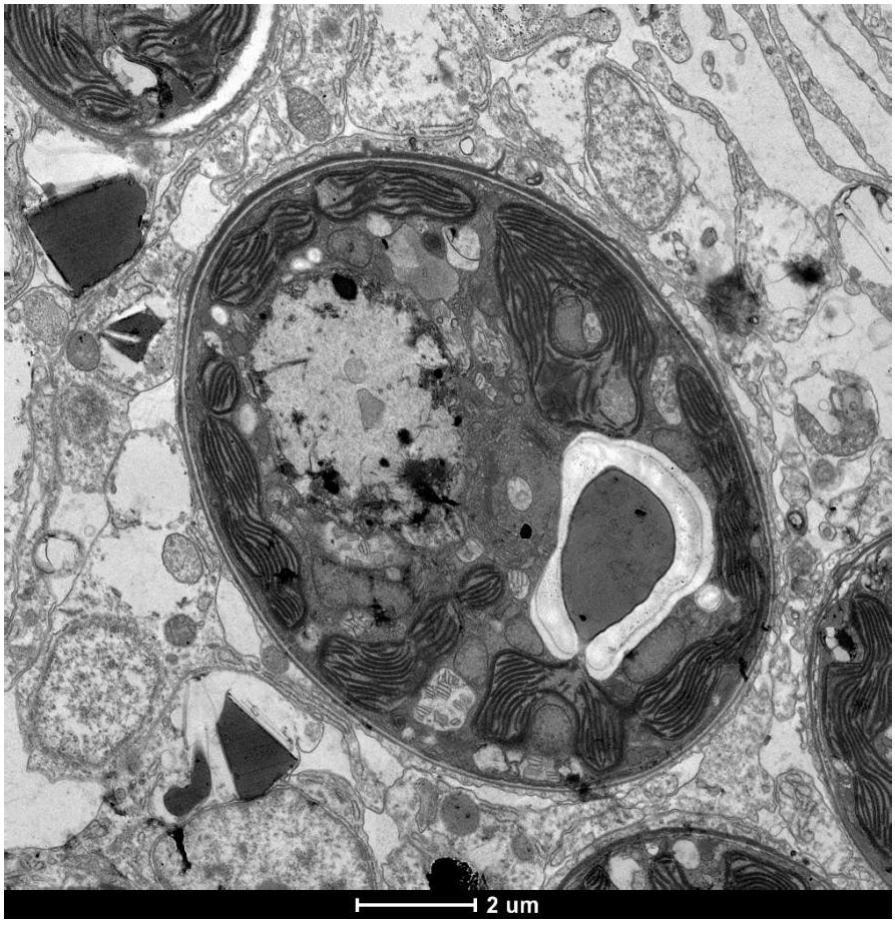

A holistic time-series analysis of stony coral tissue loss disease

Final Report

Prepared By:

Erin Papke[1]
Grace Kennedy[1]
Valerie Paul[2]
Jay Houk[2]
Neha Garg[3]
Alex Doty[3]
Michelle Heck[4,5]
Stephanie Preising[4]
Julie Meyer[6]
Allison Cauvin[6]
Yasunari Kiryu[7]
Lindsay Huebner[7]
Esther Peters[8]
Blake Ushijima[1]

[1]University of North Carolina Wilmington, [2]Smithsonian Marine Station at Fort Pierce, [3]Georgia Institute of Technology, [4]USDA Agricultural Research Service, [5]Cornell University, [6]University of Florida, [7]Florida Fish & Wildlife Research Institute, [8]George Mason University

June 15, 2025

Completed in Fulfillment of PO # C3D89C for
Florida Department of Environmental Protection
Coral Protection and Restoration Program
8000 N Ocean Dr.
Dania Beach, FL 33004

This report should be cited as follows:
{Papke E, Kennedy G, Paul V, Houk J, Garg N, Doty A, Heck M, Preising S, Meyer J, Cauvin A, Kiryu Y, Huebner L, Peters E, Ushijima B. 2024. A holistic time-series analysis of stony coral tissue loss disease. Florida Department of Environmental Protection. Florida. Pages 1-72}

This report was funded through a contract agreement from the Florida Department of Environmental Protection's (DEP) Coral Protection and Restoration Program. The views, statements, findings, conclusions, and recommendations expressed herein are those of the author(s) and do not necessarily reflect the views of the State of Florida or any of its subagencies.

Management Summary (300 words or less)

Stony coral tissue loss disease (SCTLD) is a fast-moving and deadly disease that has been devastating coral reefs in Florida and the Caribbean since 2014. Unfortunately, the causative agents have yet to be identified, which severely limits diagnostic and treatment development. To address this, we conducted a large, collaborative study using naive corals in a lab setting. These healthy naïve corals were exposed to diseased fragments, and samples were collected over time to track how SCTLD developed. The team used a wide range of scientific tools to study the transcriptome, proteome, metabolome, microbiome, and cellular ultrastructure via histology and transmission electron microscopy (TEM). We discovered that changes in the coral metabolome and microbiome occurred before any visible signs of disease appeared, suggesting that early warning signs might be detectable. Infected corals' algal endosymbionts also lost important energy reserves like starch and lipid stores, which could weaken them further. Certain bacteria became more common as the disease progressed, especially those that thrive in low-oxygen environments. Some viruses were also found in diseased corals, but it's still unclear whether they cause the disease or are just taking advantage of weakened coral animal. The study also uncovered signs of a potentially new coral disease affecting a different species, which could pose an additional threat to reef ecosystems. Overall, this project created one of the most detailed datasets ever collected on coral disease progression. It offers new insights into how SCTLD affects corals at the cellular and molecular levels and provides a valuable foundation for future research. The findings could help scientists develop early detection tools and better strategies to protect coral reefs, which are vital to marine life and coastal communities. Continued research and collaboration will be essential to fully understand and combat this complex and destructive disease.

Executive Summary (max 1 page)

As stony coral tissue loss disease (SCTLD) continues to devastate coral populations across Florida and the Caribbean, the causative agent remains unidentified. This lack of identification hinders the development of targeted treatments and reliable diagnostic tools. Despite extensive analyses across diverse sample sets, no pathogen(s) has been definitively linked to SCTLD. This may be due to the disease's complexity, potentially involving multiple microbial agents and environmental stressors, as well as variability across reefs and coral colonies. To address these challenges, this project adopted a holistic, standardized approach to sample collection and analysis. By using a consistent set of SCTLD samples across multiple analyses, we aimed to generate directly comparable datasets that could reveal patterns normally obscured by environmental variability in field samples. To minimize confounding factors, experiments were conducted in closed aquarium systems using naïve, healthy corals collected from regions before the arrival of SCTLD. The use of naïve corals also reduced the risk of pre-existing SCTLD-associated microbes in healthy tissue. Infection was induced in the lab by housing naïve corals with diseased fragments from the field. Samples were collected at five timepoints to capture the progression of disease. Each experimental tank had a corresponding control tank containing only healthy corals under identical conditions, except with a healthy fragment instead of a diseased one.

Key Findings:

Transcriptome & Proteomics: RNA virus detection tools identified hundreds of viral candidates, with 19 high-confidence viral populations found across samples. Proteomic analysis supported viral presence and helped build species-specific reference databases.

Metabolomics: Early metabolic shifts were observed in *Montastraea cavernosa* corals 48 hours post-exposure—before visible symptoms—highlighting potential biomarkers for early disease detection. Key compounds included lyso-PAF, acylcarnitines, and DGCC lipids, indicating immune and metabolic stress responses.

Histology: SCTLD was confirmed in all disease donor samples and several exposed corals. Histological markers included lytic necrosis, degraded endosymbionts, and globules from granular amoebocytes.

TEM: Diseased corals exhibited significant reductions in starch and lipid reserves, increased crystal formation, suggesting these as potential indicators of disease progression. However, the presence of viral-like particles (VLPs) did not appear to significantly correlate with health state.

Microbiome: Disease-exposed corals showed dynamic microbial shifts, with enrichment of anaerobic bacteria over time. *Vibrio coralliilyticus* was present but not dominant, suggesting a limited role in disease progression for these experiments.

Conclusions:

The dataset provides a critical baseline for future disease response and environmental stress studies. Continued integration of multi-omics data is essential to identify causative agents and biomarkers, which will be the focus for the next stages of this project. Preliminary findings also suggest the emergence of a distinct disease—*Orbicella* acute tissue loss disease (OATLD) - warranting further investigation.

TABLE OF CONTENTS

Management Summary (300 words or less) 1
Executive Summary (max 1 page) 2
Key Findings 2
Conclusions 2
TABLE OF CONTENTS 3
1. BACKGROUND 4
2. LIST OF FIGURES AND TABLES 6
2.1. Figures 6
2.2. Tables 8
3. METHODS 8
3.1. Task 1 - Quality Assurance Plan and Reporting. 8
3.2. Task 2 - Multi-Omics Analysis 8
3.3. Task 3 - Metabolomics 11
3.4. Task 4 - Histology 13
3.5. Task 5, 7, 8 - Transmission Electron Microscopy (TEM) 14
3.6. Task 6 - Microbiome Sequencing 15
4. RESULTS 15
4.1. Task 1 - Required reporting deliverables (UNCW). 15
4.2. Task 2 – Begin multi-omics analysis RNA and protein products from infected naïve corals (USDA). 18
4.3. Task 3 – Begin analysis of extracts from naive coral samples for metabolomic (SMS, GT) 25
4.4. Task 4 – Process naïve coral samples for histology and digitizing histological slides (FWC, GMU). 30
4.5. Task 5 – Embed any remaining naïve corals for TEM and image 15 more corals (UNCW) as well as analyze 10 already-imaged corals (UNCW & UPR). 39
4.6. Task 6 – Begin microbiome analysis of infected and control naive corals (UF) 44
4.7. Task 7 – Image 10 corals from DRTO and begin analyzing the imaged corals (UNCW). 48
Figure 24. A Spearman correlation matrix for the entire dataset with just the numerical parameters. Blue 51
4.8. Task 8 - Image 5 diseased *O. faveolata* samples with a potentially new coral disease observed in the Florida Keys (UNCW). 52
4.9. Host Immunity 56
Parameters measured: 56

5. DISCUSSION AND MANAGEMENT RECOMMENDATIONS 57
5.1. Discussion 57
5.2. Management Recommendations 63
6. REFERENCES CITED 65

1. BACKGROUND

Florida's Coral Reef is currently experiencing a multi-year disease-related mortality event, that has resulted in massive die-offs in multiple coral species. Approximately 21 species of coral, including both Endangered Species Act-listed and the primary reef-building species, have displayed tissue loss lesions which often result in whole colony mortality. First observed near Virginia Key in late 2014, the disease has since spread to the northernmost extent of Florida's Coral Reef, and southwest past the Marquesas in the Lower Florida Keys. The best available information indicates that the disease outbreak is continuing to spread west and throughout the Caribbean.

Previous studies, including those by our research group, confirmed SCTLD to be an infectious disease [1–3]. However, the exact etiological agent has yet to be identified. Several bacterial groups are associated with disease [4–6] while broad-spectrum antibiotics are mostly effective against disease lesions [1, 7–9]. Although, it is unclear if bacteria are initiating disease or are playing more of an opportunistic role. For example, the bacterial pathogen *Vibrio coralliilyticus* may be causing coinfections with SCTLD that exacerbate lesion progression, but pure cultures of this microbe are unable to consistently initiate disease [10]. This was an important and concerning revelation that further complicates the situation, but it allowed researchers to rule out this pathogen as a primary agent, although it remains a threat to corals.

A recent study had identified viral-like particles (VLPs) within coral tissue that were associated with the microalgae symbionts, which appeared to resemble filamentous RNA viruses [11]. The authors of that study suggested they belonged to the viral family Alphaflexiviridae based on morphology, but they did not have supporting sequencing data. Also, these VLPs were observed in both diseased and apparently healthy corals, so no connection between these VLPs and disease has yet to be established. There have been other described viruses associated with corals and their symbionts unrelated to SCTLD

[12–14]. Viruses typically outnumber bacteria in a 10:1 ratio in marine systems, so their mere presence does not provide strong evidence for their role as a primary pathogen.

The presence of these VLPs could be latent infections that manifest during host stress, which was observed in the previous viral studies [12–14]. Alternatively, they could also be an opportunistic infection that occurs after a primary agent infects, or SCTLD may be polymicrobial disease that requires infection with multiple pathogens. The latter two scenarios are observed with other coral diseases with the primary and secondary infections of *Montipora* white syndrome in Hawaii [15] and the polymicrobial black band disease [16, 17], respectively.

This project is building upon the current work of our research group, which is focusing on identifying the viruses and microbes associated with diseased corals, determining if they are specific to SCTLD lesions, and establishing if there are any associations between potential pathogens and the start of SCTLD lesions through time. This is a multi-phase project with Phase I that focused on sample collection and the beginning of sample processing. Phase II, this project, focused on samples analysis.

Project Goals and Tasks:

The goals of this project are to 1) create a comprehensive dataset from DNA, RNA, proteins, and metabolites extracted from SCTLD samples taken over time, and 2) document the cellular pathologies of SCTLD over time using histology and transmission electron microscopy (TEM). The data generated from this project will provide a comprehensive view of what is occurring during a SCTLD infection over time, as well as generate samples and data that can be used by other research groups for future analyses.

The project proposed here is a multi-phase project; the previous phase, Phase I (FY 2023 – 2024), of the project focused on sample collection and processing. Analysis of the samples was conducted in Phase II of the project (FY 2024-2025).

- **Task 1: Quality Assurance Plan and Reporting.**
- **Task 2: Begin multi-omics analysis RNA and protein products from infected naïve corals (USDA).**
- **Task 3: Begin analysis of extracts from naive coral samples for metabolomic (SMS, GT).**
- **Task 4: Process naïve coral samples for histology and digitizing histological slides (FWC, GMU).**
- **Task 5: Embed any remaining naïve corals for TEM and image 15 more corals (UNCW) as well as analyze 10 already-imaged corals (UNCW & UPR).**
- **Task 6: Begin microbiome analysis of infected and control naive corals (UF).**
- **Task 7: Image 10 corals from DRTO and begin analyzing the imaged corals (UNCW; TXST, ASU, UPR – funded separately).**
- **Task 8: Image 5 diseased *O. faveolata* samples with a potentially new coral disease observed in the Florida Keys (UNCW; NSU funded separately).**

The outcomes of this project will be incorporated into an on-going coral disease response effort which seeks to improve understanding about the scale and severity of the coral disease outbreak on Florida's Coral Reef, identify primary and secondary causes,

identify management actions to remediate disease impacts, restore affected resources, and ultimately prevent future outbreaks. As such, collaboration amongst partners is encouraged when appropriate to avoid duplication of efforts and ensure alignment of needs. Coordination with other Principal Investigators is recommended and required, as appropriate.

2. LIST OF FIGURES AND TABLES

2.1. Figures

Task 2

- Figure 1. Integrated transcriptomics and proteomics workflow for SCTLD progression analysis, and pathogen detection.
- Figure 2. A clustered heatmap showing the relative abundance of viral families (via predicted viral hits).

Task 3

- Figure 3. Alpha diversity plot of exposed to disease and control *M. cavernosa* (MCAV) fragments through different sampling periods (SP) of disease progression.
- Figure 4. Principal component analysis of healthy (HC) and SCTLD exposed (ED) *M. cavernosa* fragments over different points of disease progression (SP2: 48-hours post exposure, SP3: first visual sign of infection, SP4: 7 days after SP3, SP5: 7 days after SP4).
- Figure 5. UpSet plot of metabolite features determined to be driving differences between healthy and SCTLD exposed *M. cavernosa* fragments via SIMPER analysis (SP2: 48-hours post exposure, SP3: first visual sign of infection, SP4: 7 days after SP3, SP5: 7 days after SP4).
- Figure 6. Sunburst Plot of SIMPER Features at 48-hour Post Exposure Sampling Period (SP2).

Task 4

- Figure 7. MCAV_1081_0523TS146, recipient apparently healthy coral sample collected 8d after first exposed to disease (ED).
- Figure 8. Histological section of MCAV surface body wall, showing the gastrodermis with endosymbionts' periodic acid-Schiff's reagent (PAS) stain reaction.
- Figure 9. Histological section of mesenterial filament of MCAV_1081_0523TS146, stained with hematoxylin and eosin (H&E).
- Figure 10. Histological section of coral tissues showing gastrodermis with lytic necrosis (LN) lesions (H&E).

Task 5

- Figure 11. A bar graph showing the number of symbionts scored by health state and time point.

- Figure 12. A boxplot showing the size of the symbiont by health state over time.
- Figure 13. A boxplot showing the number (left) and size (right) of starches over time by health state.
- Figure 14. A boxplot showing the number of lipids by health state over time (left) and the size of the lipid droplets by health state over time (right).
- Figure 15. A proportion graph of the presence of crystals (left) and the area of the crystals (right) over time for each health state.
- Figure 16. A proportion graph showing the presence of VLPs within each health state at each timepoint.
- Figure 17. An NMDS incorporating symbiont area, starch size, crystal area, lipid size, number of lipids, and number of starches separated by time point.

Task 6

- Figure 18. Ordination of the principal components analysis of 49 coral microbiome samples during the experimental transmission of stony coral tissue loss disease.
- Figure 19. Dispersion of beta diversity, calculated as distance to centroid, within each health state across time.
- Figure 20. The relative abundances of 21 ASVs that were enriched in disease-exposed corals and have been previously associated with stony coral tissue loss disease.
- Figure 21. Copies of the *Vibrio coralliilyticus* vibriolysin-like *vcpA* gene per nanogram of DNA across timepoints in the experimental transmission of stony coral tissue loss disease.

Task 7

- Figure 22. Boxplots of the number of lipids (left) and size of lipids (right) over time with the health state visualized by color.
- Figure 23: A proportion graph of the percent of symbionts that have crystals by health state and time (left).
- Figure 24. A Spearman correlation matrix for the entire dataset with just the numerical parameters.
- Figure 25. A Non-metric Multidimensional Scaling plot for each timepoint showing the health states by color.

Task 8

- Figure 26. A boxplot of the number of starches by health state (left) and the size of the starches by health state (right).
- Figure 27: Boxplots of the number of lipids (left) and size of lipids (right) by health state.

- Figure 28. A proportion graph showing the presence of crystal by health state (left) and a boxplot showing the total area of the crystals by health state (right).
- Figure 29. A boxplot a of the symbiont area by health state (left) and a proportion graph of the cell symmetry by health state (right).
- Figure 30. A proportion graph showing the presence of accumulation bodies by health state (left) and a boxplot showing the size of the accumulation bodies by health state (right).
- Figure 31. A Spearman correlation matrix showing positively correlated variables in blue and negatively correlated variables in red.

2.2. Tables

Task 2

- Table 1. Reference proteomes built for pathogen detection. CNAT refers to *Colpophylla natans,* OFAV refers to *Orbicella faveolate,* and MCAV refers to *Montastraea cavernosa.*
- Table 2. The predicted viral peptide hits of various viral families in the *Orbicella faveolata* tank.
- Table 3. A subset of viral families identified that are present in the CNAT_1 (diseased donor), and OFAV2 (diseased exposed coral at timepoint 2) but not OFAV1 (healthy coral, before exposure).

Task 4

- Table 4. Sample health indicators organized by recipient species Montastraea cavernosa (MCAV) or Orbicella faveolata (OFAV) and genotype (color code) within each experimental tank, experimental time point (T) and number of days post-exposure, and sample health state.
- Table 5. Combined number (N) examined and prevalence (parenthesis) for sample health indicators.

Task 5

- Table 6. A summary of the number of coral samples imaged and symbionts scored for the 24-25 fiscal year.

3. METHODS

3.1. Task 1 - Quality Assurance Plan and Reporting.

3.1.1. There are no methods associated with this task.

3.2. Task 2 - Multi-Omics Analysis

3.2.1. RNA Sequencing

In the previous fiscal year, 61 coral fragments were shipped to Cornell University (Dr. Michelle Heck, USDA/Cornell; Stephanie Preising, Ph.D. candidate) for parallel RNA extraction and sequencing, DNA extraction, (Task 6, University of Florida) and proteomics. The raw RNA-seq FASTQ files were sent to Matt Sulivan, Ohio State University and Dawson Phan, Ph.D. student at Ohio State University, via GLOBUS.

RNA virus discovery is challenging due to a lack of standards in the field at every level, from sampling to bioinformatic processing to data analysis [18]. Currently, RNA viruses are identified through their hallmark gene, RNA-dependent RNA polymerase (RdRP) which has a highly conserved protein structure but also exhibits substantial evolutionary and sequence divergence [19]. Typically, the identification of an RdRP sequence is done by assessing protein sequence similarities through Hidden Markov Models (HMMs) [18] and iterative rounds of curation.

The Sullivan lab has developed a workflow that identifies RdRP-encoding sequences through an iterative, competitive HMM-search method, benchmarked with data from the global oceans [20]. This method, here referred to as "RdRP-Search", excels at identifying divergent RdRP sequences but is highly conservative, resulting in fewer identified but higher confidence RdRP encoding viral populations compared to other tools. geNomad is another viral identification tool that uses a mix of sequence feature annotations and neural networks to detect sequence patterns that identify DNA viruses, plasmids, and RNA viruses [21]. One benefit to using geNomad is that it can identify RNA viruses with or without RdRP genes. While this may be valuable in identifying other segments of RNA viruses that are not on the RdRP encoding sequence, the RNA virus sequences lacking RdRP genes are challenging to curate as true or false RNA viruses.

Our first goal is to identify as many RNA viruses as possible to search for possible viral pathogens in corals afflicted by SCTLD. Here we run both RdRP-search and geNomad to compare the resulting predictions with the goal of determining a best practices approach to deploy either or both approaches tandemly. This approach will then be used in establishing the final dataset for RNA viral analysis.

Bioinformatic Methods:

RdRP-Search

After an initial read quality control and assembly for each sample, proteins were predicted using transeq (EMBOSS:6.6.0.0). These proteins served as the input for RdRP-Search [20]. Briefly, RdRP-search searches the predicted proteins against a database of RdRP HMM profiles from 11 studies [19, 22–25, 25–30] and NCBI's GenBank using hmmsearch (HMMER v3.3) with a bitscore of at least 30, and alignment fraction of at least 0.7. The resulting HMM profiles are then trimmed (hmmsearch option -A), clustered with MCL (-I 2.0), aligned with MUSCLE, and used to update the HMM database with new RdRP profile HMMs from our data using hmmbuild. After 10 iterations of this process, putative trimmed RdRP domain sequences are then searched against a competitive database of RdRP and non-RdRP HMM profiles to remove false positive RdRP domains and obtain a set of curated, conservative RdRP-containing contigs.

geNomad

For RNA virus identification using geNomad [21], the software was run using default arguments and databases. Based on taxonomic annotations generated from geNomad, RNA virus contigs were separated by filtering for virus realm "*Riboviria*" (see geNomad [21] for methods details).

Plans for comparing RdRP-Search and geNomad

To compare the RNA virus detection capabilities of RdRP-Search and geNomad, we will be using a "positive" dataset (sequences identified as RNA viruses from the curated Riboviria Metatranscriptomics (RVMT) database [31]) and a "negative" dataset (sequences identified as non-RNA viruses also from Neri et al. 2022 [31]). Using these datasets, we can compare the true positive and false positive rates as well as specific parameter thresholds for both geNomad and RdRP-search to establish the best approach for RNA virus identification in this data. We will also compare the overlapping and exclusive vOTUs identified from each pipeline. Additionally, for RNA viruses without RdRP genes identified by geNomad, we will manually curate the populations based on a set of markers associated with RNA viruses developed by geNomad [21].

Read mapping

Prior to read mapping for predicted RNA virus quantification, polyadenylated-tails were removed from both the reads and the RNA viral sequences through consecutive trimming from the left and right of the sequence using bbduk (39.06) (hdist=2, k=10, restrictright or restrictleft = 20, minlength=30). A final polyadenylation removal was conducted also using bbduk (39.06) (trimpolya=3, minlength=30). Resultant non-polyadenylated RdRP-encoding contigs were then clustered with CheckV-0.8.1 at 90% ANI and 80% TCOV to establish virus operational taxonomic units (vOTUs).

Non-polyadenylated reads were mapped against the NON-CLUSTERED RdRP-encoding contigs using bowtie2 (v. 2.4.4) using parameters -q --local -D 20 -R 3 -N 0 -L 16 -i S,1,0.50 -p 40 -I 0 -X 2000 --no-unal –non-deterministic. Resultant BAM files were used as mapping coordinates for CoverM (v.0.6.1-3) with parameters --min-read-percent-identity .90 --min-read-aligned-percent .75 -m trimmed_mean. For RdRP-search, coverages for each contig per vOTU were then summed to derive a vOTU coverage value, which was then normalized by the sequencing depth per sample to simulate a proxy for viral relative abundance. For geNomad, coverages for each contig per vOTU were taken as a trimmed mean and normalized by sequencing depth per sample to simulate viral relative abundance.

3.2.2. Proteomics

In the previous fiscal year, 61 coral fragments were processed for proteomics. The protein extracts were generated from each sample in the last fiscal year, and an initial data-dependent acquisition (DDA) was performed on a pooled digest using gas-phase fractionation to both assess overall digest quality and stabilize chromatographic retention times on a new column. For quantitative analyses, individual samples were analyzed by data-independent acquisition (DIA) using a wide-isolation window method (Dora_neo_150u_15cm_8mzov_400–1000_60m), while pooled samples were

interrogated with a series of narrow-isolation DIA methods (e.g., Dora_neo_150u_15cm_4mzov_500–600_60m), each covering a 100 m/z precursor range (400–500, 500–600, etc.). Raw files were named according to the convention "D_<YYYY_MMDD><*OperatorInitials*><RunOrder>_<TubeID>" (e.g., D_2024_0130_RJ_16_14), and an accompanying CSV metadata file recorded the instrument method and sample annotations (files attached in the hard drive). System performance was monitored throughout the acquisition by periodic injections of a bovine serum albumin (BSA) digest spiked with the Thermo PRTC peptide standard.

Additionally, the 61 raw RNA-seq FASTQ files generated by Illumina high-throughput sequencing (included in the hard drive) were used to construct species-specific meta transcriptomes with Trinity, performing separate assemblies for each coral species and for each species–timepoint combination (e.g., Species1_Timepoint1). The raw and assembly files have been deposited on the project hard drive for record-keeping and downstream use. The sequence redundancy is being reduced using the MMSQ2 and Vsearch tools, and predicted coding sequences via TRANSdecoder/ANGEL are being extracted from these transcriptomes to generate draft proteomes. Finally, non-redundant proteome sequences are being organized into custom bacterial and viral protein databases, which will serve as reference libraries for our subsequent metaproteomic and viral detection workflows. The predicted viral peptides will be ran against blastp's viral database.

3.3. Task 3 - Metabolomics

Coral fragments/polyps were extracted and lyophilized at Smithsonian Marine Station (SMS) then shipped to Georgia Institute of Technology for metabolomic analysis. Dried extracts (5 mg) were resuspended in 250 µL of 100% MeOH containing 1µM sulfadimethoxine as internal standard. The samples were diluted 1:10 in 100% MeOH prior to LC-MS/MS analysis via Thermo Fisher Vanquish UHPLC equipped with a Kinetex 1.7 µm C18 reverse phase UHPLC column (50 × 2.1 mm) coupled to Thermo Fisher Exploris 240 mass spectrometer equipped with an electrospray ionization (ESI) source. Reverse phase chromatography was carried out using two mobile phases, mobile phase A: H_2O + 0.1% v/v formic acid, and mobile phase B: ACN + 0.1% v/v formic acid. The gradient applied for chromatographic separation was 5% solvent B and 95% solvent A for 3 minutes, a linear gradient of 5%B to 35%B over 2 minutes, a linear gradient increase from 35%B to 95%B over 15 minutes, held at 95%B for 4 minutes, a linear decrease from 95%B to 5% B over 0.1 minutes, and held at 5%B for 1.9 minutes. A mixture of six compounds (amitriptyline, coumarin-314, sulfachloropyridazine, sulfadimethoxine, sulfamethazine, and sulfamethizole) was injected every 8 samples to monitor column and instrument performance throughout the data acquisition.

The eluent was introduced to the Exploris 240 mass spectrometer by electrospray at 3.5 kV, and data was acquired in positive polarity mode. Sheath gas, auxiliary gas, and sweep gas were set at 50, 10, and 1 (arbitrary units) respectively throughout data acquisition. The ion transfer tube was set at 325 °C and the vaporizer temperature was set at 350 °C. Expected peak width was set at 6 seconds and advanced peak determination and EASY_IC™ was selected. MS^1 Data were acquired over a mass range of 150-1500 *m/z* with a resolution of 120,000, and AGC target was set to standard. Features were selected for MS^2 fragmentation in a data dependent manner. The top MS^1 features in the chromatographic peak were selected for fragmentation in the HCD cell (normalized collision energy 10%, 30%, 60%), after which they were dynamically excluded from additional

fragmentation. MS^2 Spectra were acquired at 30,000 resolution with AGC target set to standard, maximum injection time set to auto, and 1 microscan. Data were centroided and converted to mzXML format using MSConvertGUI version 3.0 (prior to processing with MZmine3 version 3.1.0. The data were preprocessed using mass detection, ADAP chromatogram builder, baseline resolver, ^{13}C isotope filter, join aligner, duplicate peak filter, and feature list rows filter. The data were exported into tabular and mascot generic format (MGF) for processing with Global Natural Products Social Molecular Networking (GNPS) Feature-Based Molecular Networking (FBMN) workflow[1]. The outputted tabular data, referred to as quant table, contains samples in columns and features in rows. Each feature is assigned an *m/z* value, retention time, and unique numerical identifier. At the completion of the GNPS job, FBMN was imported to Cytoscape version 3.8.2 for visualization and analysis of molecular network.

SIRIUS (version 5.7.2) with CSI:FingerID and CANOPUS[2] was used to perform *in silico* annotations and compound class discovery, respectively. CSI:Finger ID was employed using default settings and all databases selected. After computation of fragmentation tress from acquired data, the chemical formulas and structures were ranked by machine learning to determine which structure best matched the acquired data. CANOPUS takes the output of the CSI:FingerID workflow and predicts chemical classes based on molecular fingerprints.

Blank subtraction was performed on quant table using Jupyter notebook prior to statistical analyses (available on GitHub: https://github.com/Garg-Lab/SCTLD-Time-Series). The mean of each feature from samples was compared to the mean of each feature from the solvent controls and UPLC-MS blanks. If the mean of each feature in the samples was greater than 0.25× the mean of each feature in the blanks, then that feature was retained. At the end of the script, the quant tables are exported with blank subtracted values for each feature and an additional column containing "TRUE" if the feature was retained and "FALSE" if the feature was not.

A Bray-Curtis similarity matrix was generated from the .qza file output of the GNPS FBMN job via qiime2 metabolomics plugin (GitHub: https://github.com/mwang87/q2_metabolomics). The output of this workflow was used to generate alpha-diversity plots of healthy and SCTLD exposed *M. cavernosa* fragments through all experimental sampling periods.

Methods for disk diffusion assays of the extract partitions from corals exposed to SCTLD over time.

Glycerol stocks of the pathogenic challenge strain *Vibrio coralliilyticus* OfT6-21 were revived onto seawater agar (SWA) (4 g tryptone, 2 g yeast /L seawater) and grown overnight at 28 °C. The morning of each assay, 4 ml of seawater broth was inoculated with three colony forming units and grown at 28 °C and 200 rpm. For testing, the culture was adjusted to OD600 0.50 +/- 0.05 (Thermoscientific Genesys 180 UV-Vis Spectrophotometer) and 200 µl was added to each 150 mm seawater agar (SWA) plate. The inoculum was dispersed with sterile beads and left to dry for 15 minutes prior to administering treatment disks to the SWA plate.

Some of the extract partitions were assayed at a range of concentrations, and 15 µg/disk was found to produce measurable results that were not too large to interpret. To ensure accuracy, each sample was resuspended and transferred to a freshly weighed vial. The EtOAc and BuOH partitions were completely dissolved in methanol. Each sample was transferred via glass pipet to a prewashed 7 ml scintillation vial (MeOH 3x) and dried in vacuo at 35 °C (ThermoScientific Savant SPD121P SpeedVac concentrator).

Each EtOAc or BuOH partition sample was resuspended to 0.75 mg/ml and 20 µl was administered to each disk (Thermoscientific remel blank paper disks Cat. # R55054) and allowed to dry under a sterile laminar flow hood for 30 minutes. Solvent controls were prepared in tandem and 62.5 µg/ disk of nalidixic acid was prepared as a positive control. Disks were applied treatment side down to the SWA plate. The assay was incubated for 24 hours at 28 °C prior to scoring the zones of inhibition (ZOI) around each paper disk on the plate, which was measured from edge of the disc to edge of the ZOI. The ZOI of the methanol control was subtracted from the treatment ZOIs in a plate specific manner.

3.4. Task 4 - Histology

Gross Observations
After the fixed specimens were received at FWRI, the external surface of each coral fragment was photographed using a digital camera (JENOPTIK GRYPHAX, Jena, Germany) attached to a dissecting microscope (LEICA M125, Wetzlar, Germany) to identify tissue-loss lesions. The presence or absence of mesenterial filaments protruding on the surface of the tissue and of heterotrich ciliates (*Halofolliculina*) on the skeleton were also examined. The fragment was then placed in a solution of 10% ethylenediaminetetraacetic acid (EDTA), adjusted to neutral pH, and decalcified [32]. After the skeleton was removed, both gross external and internal surface views were reexamined with a dissecting microscope and photographed. Any tissue abnormalities of the samples observed at this step were noted; for example, some samples exhibited protrusion of mesenterial filaments, and images of both oral and aboral views were recorded.

Histology
Microscopic lesions in samples of CNAT, MCAV, and OFAV used in this study were identified and described using the parameters for diagnosing SCTLD as originally described by Landsberg et al. (2020) and published in the U.S. Geological Survey Case Definition [33]). These lesions included lytic necrosis of the polyp/coenenchyme's surface body wall gastrodermis associated with degenerative changes in the endosymbionts, including cytoplasmic deformity, cytoplasmic vacuolation, and the presence of enlarged or lysed symbiosomes, as well as necrosis and loss of the endosymbionts, necrosis of epithelial cells, and abnormal staining and degradation of the mesoglea. Other observations, including atrophy of the epidermis or gastrodermis; presence of hypertrophied mucocytes; degraded granular amoebocytes; gastrodermis or calicodermis detaching from the mesoglea; microorganisms, such as endolithic fungi and algae, ciliates, and rod-shaped (bacilloid-like), spherical (coccoid-like), or coccobacilloid-like structures (suspect bacteria), and corallicollids (apicomplexans) were also recorded in an Excel spreadsheet.

Because the Giemsa stain is useful for identifying foreign organisms, including suspect bacteria, we re-sectioned in Year 2 the previously prepared paraffin blocks of all samples and stained them with Giemsa at FWRI [34]. All the paraffin-embedded tissue blocks except for two (one lost MCAV block specimen, project ID #0523TS081, health state ED; and one dead CNAT specimen, project ID #0523T281, health state DD) were

duplicated and stained with the Giemsa procedure. One complete set of Giemsa-stained slides was sent to GMU, while the other set remained at FWRI. YK and LH examined the Giemsa-stained slides for foreign organisms and compared the findings with those from the Mayer's hematoxylin and eosin (H&E; [35]), periodic acid–Schiff–metanil yellow (PAS-MY; [36]), and thionin [35] stained slides.

From November 2024 through June 2025, GMU and FWRI held routine weekly teleconference meetings to discuss the experiment, preliminary histopathological findings, data recording and analysis protocols, and slide imaging plans.

Histoslide Digital Scanning
When most of the histoslide examinations were completed, selected slides from adjacent serial sections for all but two of the blocks—stained with H&E, thionin, Giemsa, and PAS-MY—were digitized during the late third quarter into the fourth quarter of this study. These histoslides were shipped to and scanned by a service vendor, iHisto (Salem, MA), arranged by GMU. The vendor then checked the quality of the digitized images in the files (in the format ".svs") and posted them in folders for downloading by FWRI's SCTLD Data Management Staff. The files were then uploaded to FWRI's eSlide Manager system (a virtual microscope collection) for use by other coral pathologists and for educational training purposes. The files are now available at https://myFWRI.com/research/about/resources/eslide/, and free access can be requested using the form on that webpage. The digitized histoslides can be examined by the free software Aperio ImageScope provided in the eSlide Manager system (also available for download with User Guide from https://www.leicabiosystems.com/us/digital-pathology/manage/aperio-imagescope/) or the newer free software SlideViewer (available for download with Users Guides from https://www.ihisto.io/digital-histology). After GMU checked the histoslide files and file names, the original histoslides were returned to GMU and FWRI, respectively, to retain these copies of the glass slides for further study. The metadata for this collection will also be provided to users.

3.5. Task 5, 7, 8 - Transmission Electron Microscopy (TEM)

All TEM samples were fixed utilizing the same protocol as previously described [32]. Briefly, coral samples were fixed in a combination of paraformaldehyde and glutaraldehyde in Instant Ocean and maintained in the fixative in 4°C until the secondary fixation. After the primary fixation, the coral tissue was washed in a series of buffers, secondarily fixed in osmium tetroxide, and dehydrated in a series of ethanol concentrations before being embedded in Spurr's resin. The embedded tissue was sectioned to 90 nm using an ultramicrotome, placed on formvar coated copper grids, and post-stained with UranyLess and lead citrate. The sections were imaged using the FEI Tecnai Spirit Bio-Twin Transmission Electron Microscope with a CCD camera at the Richard M. Dillaman Bioimaging Facility at UNCW.

Each sample was given a unique identifier to eliminate imaging and analysis bias and images were analyzed using ImageJ (version Java 1.8.0_345) [37]. The scale was set using the individual scale bar from each micrograph. Approximately 26 metrics within the symbionts were scored, including signs of cellular breakdown, number and size of

storage granules, membrane integrity, and the presence of viral-like particles (VLPs). Each metric along with identifying factors such as time point, health state, and coral species, were analyzed in RStudio. Kruskal Wallis and pairwise Dunn tests were performed on continuous parameters and the Fisher's exact test was used for categorical parameters with the Bonferroni p adjustment method for the Dry Tortugas and *Orbicella* samples and the BH method for the Time Series samples.

3.6. Task 6 - Microbiome Sequencing

Extracted DNA of 61 samples from Task 2 was sent to UF from USDA for microbiome analysis in the previous fiscal year. We characterized the bacterial community through 16S rRNA gene libraries (V4 region) as previously described (Meyer et al., 2019). Illumina sequencing of the libraries was performed at the University of Florida Interdisciplinary Center for Biotechnology Research NextGen DNA Sequencing Core Facility (RRID: SCR_019152) on an Illumina MiSeq with the 2 x 150 base pair (bp) v. 2 cycle format. Cutadapt was used to remove primers and Illumina adaptors, and amplicon sequence variants (ASVs) were called using the DADA2 bioinformatic pipeline with the SILVA v138.1 database. ASVs classified as mitochondria or chloroplast were removed from the dataset. Data analysis was performed in R with packages such as phyloseq, vegan, DESeq2, using established methods (https://github.com/meyermicrobiolab).

In addition, we quantified the abundance of the coral pathogen *Vibrio coralliilyticus* using droplet digital PCR (dPCR) services at the University of Florida Interdisciplinary Center for Biotechnology Research Gene Expression and Genotyping Core (RRID: SCR_019145) for droplet formation, amplification with EvaGreen master mix, and analysis with the BioRad QX200 Droplet Digital PCR system.

4. RESULTS

4.1. Task 1 - Required reporting deliverables (UNCW).

4.1.1. The files for the corresponding tasks are listed below:

4.1.1.1. **Task 1:** Required reporting deliverables (UNCW).

1) Manager-level summary.
   - The summary was included at the beginning of this report.
2) Meta-data uploaded to DataOne.
   - Confirmation email *DataOne Upload Approval Email.pdf* included with the final report.
   - Have included *Time Series Experiment Sample list (general).xlsx* which is the main list of all samples originally collected for this project.
3) Separate folder with a smaller subset of photos that highlight the project.

- File with *Subset of Photos of Project.pptx* emailed to DEP with final report.

4) Final report 508-complian (PDF and Word).
   - Word and PDF documents *Ushijima et al. 2025 DEP CRP Final Report* document email to DEP.
5) Final presentation to the Disturbance Advisory Committee (DAC) and/or other DEP approved body.
   - Final presentation was giving on May 14, 2025 to the DAC and the final presentation file *5.14.2025 Times Series Final DAC.pdf* was included with the final report email to DEP.

4.1.1.2. **Task 2:** Multi-Omics (USDA/Cornell, OSU).

1) An excel sheet generally outlining the processing of each sample.
   - File *Task_2_Samples.xlsx* provided with the final report.
2) 61 de novo draft transcriptomes, full dataset sent to DEP using a physical drive or cloud storage.
   - This dataset was included in the physical drive sent to DEP. Please see *Task2_Hard_drive_file_explanation.docx*
3) 61 draft proteomes, full dataset sent to DEP using a physical drive or cloud storage.
   - This dataset was included in the physical drive sent to DEP. Please see *Task2_Hard_drive_file_explanation.docx*
4) 61 virome profiles from the transcriptomes, full dataset sent to DEP using a physical drive or cloud storage.
   - This dataset was included in the physical drive sent to DEP. Please see *Task2_Hard_drive_file_explanation.docx*
5) A viral and bacterial peptide profile from proteomes drafted in Q2 with dataset sent to DEP using a physical drive or cloud storage.
   - This dataset was included in the physical drive sent to DEP. Please see *Task2_Hard_drive_file_explanation.docx*
6) Results from digital droplet PCR of putative viral sequences with the dataset sent to DEP using a physical drive or cloud storage.
   - A equivalent dataset was developed from the transcriptomics data, which is more informative and accurate than PCR. This was included in the physical drive. Please see *Task2_Hard_drive_file_explanation.docx*.

4.1.1.3. **Task 3:** Metabolomics (SMS, GT).

1) Excel sheet detailing progress on extracts and antibacterial test results.

- Documented in file *Task_3_Extracts_Antimicrobial.xlsx* provided with the final report.

2) Deposition of metabolomics data to public data repository, namely MassIVE. A dataset id and weblink will be provided for access to the data.
   - Raw data files acquired in positive ionization mode were uploaded to the mass spectral repository MassIVE and are available at https://massive.ucsd.edu under the identifier MSV000094526.
3) Inventory of metabolite features that differentiate over time based on health state.
   - Documented in the file *Task_3_Sample_Analysis.xlsx* provided with the final report.
4) Annotation of identity and sources of these compounds when available.
   - Documented in the file *Task_3_Sample_Analysis.xlsx* provided with the final report.
5) Annotation of chemical class of these metabolites in absence of compound annotation.
   - Documented in the file *Task_3_Sample_Analysis.xlsx* provided with the final report.

4.1.1.4. **Task 4:** Histology (FWC, GMU).

1) An excel sheet generally outlining the processing of each sample.
   - Documented in the file *Task_4_Sample_Processing.xlsx* included with the final report.
2) Interpret and diagnose all samples from the naïve transmission experiment with results recorded in an Excel file; these results will be summarized in the final report shared with DEP.
   - Included with final report.
3) Checklist of digitized slides.
   - Documented in the file *Task_4_Digitized_Slides.xlsx* included with the final report.
4) Upload digitized slide files to FWC-FWRI's eSlide Manager system.
   - FWC-FWRI has worked with the DataOne team and have made the slides available upon request from https://myfwc.com/research/about/resources/eslide/

4.1.1.5. **Task 5:** TEM (UNCW).

1) Excel document of all existing samples to date, including location of samples, and the products obtained from each sample.
   - Documented in the file *Task_5_7_8_samples.xlsx* included with the final report.
2) Representative TEM images from at least 15 corals.

- Uploaded to the DataOne entry for this project.
- Also included as a OneDrive link sent with this report.

3) Complete analysis of 10 already-imaged corals as an excel documents with scored metrics .

4.1.1.6. **Task 6:** Microbiomes (UF).

1) Excel document of all existing samples to date, including location of samples, and the products obtained from each sample.
2) Excel spreadsheet with dPCR assay results.
3) All raw data associated with task.

4.1.1.7. **Task 7:** TEM – DRTO (UNCW)

1) Excel document of all existing samples to date, including location of samples, and the products obtained from each sample.
   - Documented in the file *Task_5_7_8_samples.xlsx* included with the final report.
2) Representative TEM images from at least 10 corals.
   - Uploaded to the DataOne entry for this project.
   - Also included as a OneDrive link sent with this report.
3) Complete analysis of 10 already-imaged corals as an excel documents with scored metrics.
   - Documented in the file *Task_7_analysis.xlsx* included with the final report.

4.1.1.8. **Task 8:** TEM – OATLD (UNCW).

1) Excel document of all existing samples to date, including location of samples, and the products obtained from each sample.
   - Documented in the file *Task_5_7_8_samples.xlsx* included with the final report.
   - Documented in the file *Task_8_analysis.xlsx* included with the final report.
2) Representative TEM images from at least 5 corals.
   - Uploaded to the DataOne entry for this project.
   - Also included as a OneDrive link sent with this report.

4.2. Task 2 – Begin multi-omics analysis RNA and protein products from infected naïve corals (USDA).

4.2.1. RNA Sequencing

From RdRP search, a total of 23 vOTUs were identified (which all have RdRPs), all but one of which were found in only a single sample according to read recruitment. This decreases the statistical power associated with the RdRp-search results. From geNomad, a total of 396 vOTUs were identified, 131 of which have RdRPs and 265 do not. A majority of the geNomad predicted vOTUs could be found in multiple samples,

allowing for much greater statistical power. 19 vOTUs were identified by both geNomad and RdRP-search, alluding to high-confidence in these viral populations identified.

4.2.2. Proteomics

Data-dependent acquisition (DDA) of a pooled coral digest, fractionated in the gas phase, yielded broad peptide coverage, initial injections exhibited minor retention-time drift that narrowed over successive runs, stabilizing chromatographic performance by the fourth fraction. A comprehensive metadata log (.csv) captured each raw file name (e.g., D_2024_0130_RJ_16_14), instrument method, and sample comment to ensure full traceability. Downstream data-independent acquisition (DIA) employed two approaches, a wide-window method (8 m/z over 400–1000 m/z) for individual samples, and sequential narrow-window method (4 m/z over contiguous 100 m/z segments) on pooled material. Repeated reinjections of the pooled digest with the wide-window DIA protocol demonstrated highly consistent peptide signal intensities, and periodic system-suitability check using a bovine serum albumin (BSA) digest spiked with the Thermo PRTC standard confirming the stable mass accuracy and retention-time reproducibility throughout the entire acquisition.

From the 61 Illumina-derived RNA-seq FASTQ files, we generated *Colpophylla natans* CNAT and *Orbicella faveolata* OFAV mega meta transcriptome assemblies with Trinity. The MCAV mega meta transcriptome is in process, due to the nature of the large computationally intensive datasets the transcriptome has not been finished at time of report submission. From there, we are performing separate de novo assemblies for each coral species and for each species timepoint combination (e.g., “SpeciesX_TimepointX”). These predicted proteins will serve as references for the proteome data collected, and aid in building custom bacterial and viral protein databases, serving as comprehensive reference libraries for our subsequent pathogen detection pipelines.

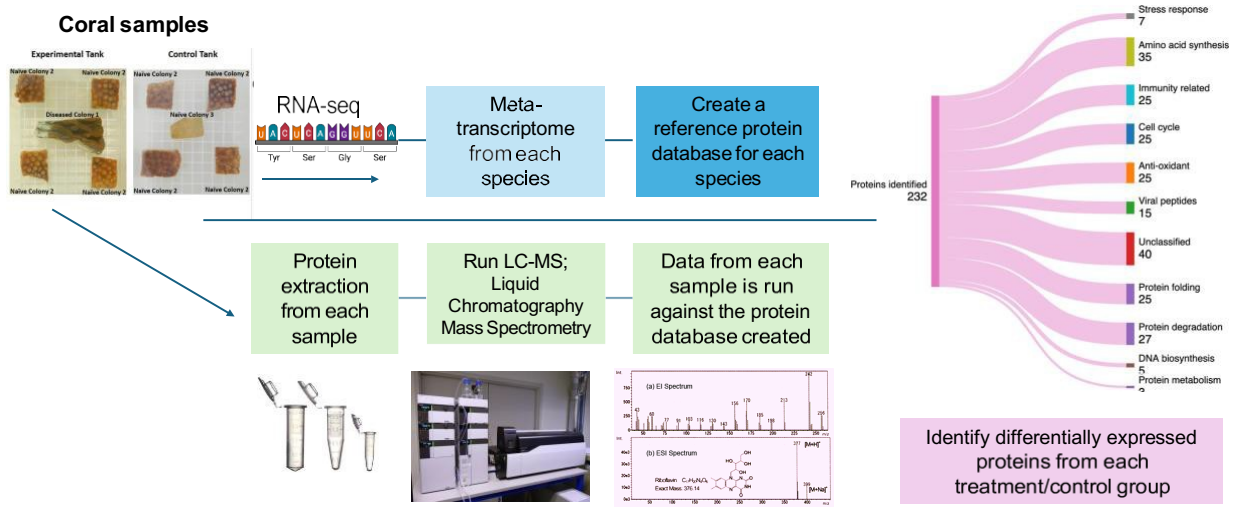

Figure 1. Integrated transcriptomics and proteomics workflow for SCTLD progression analysis, and pathogen detection. The coral specimens from each species were subjected to high-throughput RNA sequencing to generate species-specific meta-transcriptome assemblies, from which predicted coding sequences were compiled into custom protein reference databases. Parallel protein extractions from individual samples were analyzed by LC-MS, and resulting spectra were searched against the tailored databases. The downstream comparative analysis of spectral matches will enable the identification and quantification of transcripts, proteins of the corals, and pathogens that are differentially expressed between treatment and control groups.

Table 1. Reference proteomes built for pathogen detection. CNAT refers to *Colpophylla natans,* OFAV refers to *Orbicella faveolate,* and MCAV refers to *Montastraea cavernosa.*

Reference transcriptome/proteome built	**Sample ID included:**	**Status**
CNAT all	All CNAT samples	Complete
OFAV all	All OFAV samples	Complete
MCAV all	All MCAV samples	*In progress*
MCAV_pre_experiment_timepoint1	0523TS004, 0523TS009, 0523TS009, 0523TS019	Complete
OFAV_pre_experiment_timepoint1	0523TS024	Complete
CNAT _diseased_timepoint1	0523TS029, 0523TS034, 0523TS039, 0523TS044,0523TS044, 0523TS104	*In progress*

MCAV_timepoint2	0523TS054, 0523TS059, 0523TS064, 0523TS069, 0523TS074, 0523TS079 0523TS084, 0523TS089, 0523TS094	*In progress*
OFAV_timepoint2	0523TS099, 0523TS074	Complete
MCAV_timepoint3	0523TS109, 0523TS114, 0523TS119, 0523TS124, 0523TS134, 0523TS139 0523TS144, 0523TS149	*In progress*
OFAV_timepoint3	0523TS154, 0523TS129	Complete
MCAV_timepoint4	0523TS184, 0523TS189, 0523TS194, 0523TS159, 0523TS204, 0523TS209 0523TS214, 0523TS164	*In progress*
OFAV_timepoint4	0523TS199, 0523TS219	Complete
MCAV_timepoint5	0523TS169, 0523TS174, 0523TS179, 0523TS224, 0523TS229, 0523TS234 0523TS239, 0523TS244, 0523TS249, 0523TS254, 0523TS264, 0523TS269 0523TS289	*In progress*
OFAV_timepoint5	0523TS259, 0523TS279, 0523TS309	Complete
CNAT_diseased_timepoint5	0523TS294, 0523TS299, 0523TS304	*In progress*

Table 2. The predicted viral peptide hits of various viral families in the *Orbicella faveolata* tank. Headers 'Virus/Virus family' indicates the predicted virus / virus family hit, 'CNAT (diseased) in tank' indicates the number of hits in the *C. natans* diseased fragment in the tank, 'OFAV timepoint 1 (HH)' indicates the number of hits to a virus/viral family of the *O. faveolata* healthy coral at timepoint 1, before disease was introduced, and 'OFAV Timepoint 2 (exposed to disease)' indicates the number of hits to the *O. faveolat*a coral exposed to disease at timepoint 2.

Virus / Virus family	CNAT (diseased) in tank	OFAV Timepoint 1 (HH)	OFAV Timepoint 2 (exposed to diseased
Flamingopox virus FGPVKD09	69	61	103
Tetraselmis virus 1	68	60	104
Only Syngen Nebraska virus 5	68	60	104
Chlorovirus heliozoae	68	60	104
Chrysochromulina ericina virus	67	60	105

Canarypox virus	67	59	103
Tupanvirus soda lake	67	58	99
Tupanvirus deep ocean	67	58	99
Paramecium bursaria Chlorella virus NY2A	64	58	100
Noumeavirus	66	59	96
Brazilian marseillevirus	65	59	96
Lausannevirus	65	58	95
Micromonas pusilla virus SP1	61	58	97
Tokyovirus A1	60	57	92
Mythimna separata entomopoxvirus 'L'	60	57	92
Micromonas pusilla virus 12T	60	52	91
Yellowstone lake phycodnavirus 1	63	52	86
Betaentomopoxvirus amoorei	54	52	88
Cryptophlebia peltastica nucleopolyhedrovirus	50	50	85
Adoxophyes orana nucleopolyhedrovirus	50	49	76
Choristoneura biennis entomopoxvirus	50	47	76
Adoxophyes honmai nucleopolyhedrovirus	47	45	72
Hemileuca sp. nucleopolyhedrovirus	46	41	69
Euproctis digramma nucleopolyhedrovirus	39	44	73
Choristoneura rosaceana entomopoxvirus 'L'	48	42	66
Hyposidra talaca nucleopolyhedrovirus	48	40	67
Malacosoma neustria nucleopolyhedrovirus	41	41	72
Tunisvirus fontaine2	37	41	73
Sucra jujuba nucleopolyhedrovirus	49	28	57
Lambdina fiscellaria nucleopolyhedrovirus	35	41	58
Erannis ankeraria nucleopolyhedrovirus	36	27	56
Shrimp hemocyte iridescent virus	37	24	49
Golden Marseillevirus	37	23	50

Cherax quadricarinatus iridovirus	37	24	49
Buzura suppressaria nucleopolyhedrovirus	35	24	51
Megavirus chiliensis	28	19	46
Megavirus baoshan	28	19	46

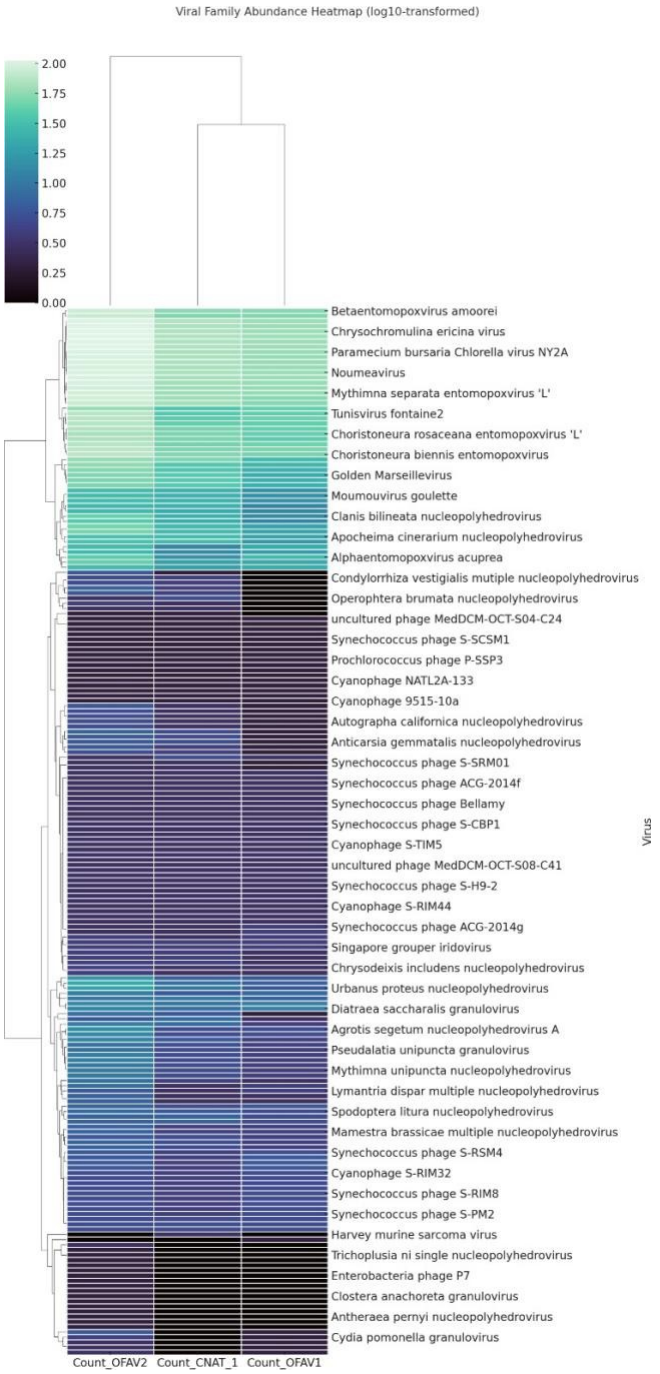

Figure 2. A clustered heatmap showing the relative abundance of viral families (via predicted viral hits). Hits from across three samples, CNAT_1, OFAV1, and OFAV2. CNAT 1 corresponds to sample ID 0523TS049, the diseased donor coral fragment placed in tank 5E, OFAV1 corresponds to sample ID 0523TS024, the healthy coral fragment sampled at timepoint 1 before disease exposure, and OFAV2 corresponds to sample ID 0523TS099, the coral fragment exposed to disease at timepoint 2. The viral family counts were obtained through BLASTP homology searches of predicted protein sequences against a custom viral protein database, followed by high-confidence filtering (>85% identity and an e-value of < 1e-10). The counts were log-transformed to improve visualization of abundant and low abundant viral families. Hierarchical clustering was applied to viral families and samples to show patterns of similarity and divergence in viral community composition.

Table 3. A subset of viral families identified that are present in the CNAT_1 (diseased donor), and OFAV2 (diseased exposed coral at timepoint 2) but not OFAV1 (healthy coral, before exposure). These include baculovirus (predominantly arthropod-associated viruses, but at relatively low hits.

Virus	CNAT_1	OFAV 1	OFAV2
Operophtera brumata nucleopolyhedrovirus	4	0	2
Plutella xylostella granulovirus	3	0	6
Phthorimaea operculella granulovirus	3	0	5
Condylorrhiza vestigialis multiple nucleopolyhedrovirus	3	0	4
Choristoneura fumiferana DEF multiple nucleopolyhedrovirus	3	0	4

DATASET file explanation (hard drive contents sent to FL DEP):

/RNA SEQ data:

- Raw files: The raw FASTQ files used to generate transcriptomes
- Transcriptomes: The built transcriptomes of each individual coral sample
- DEP Report materials: Files from the transcriptome data, viral ID searches
    - [IDMethodUsed] = geNomad or RdRP-Search
    - [IDMethodUsed]-Abundance-Table-Norm.csv
    - A table of abundances for identified RNA viruses in the data in CSV format
    - [IDMethodUsed]-Abundance-Table-Norm.txt
    - A table of abundances for identified RNA viruses in the data in TXT (white-space delimited) format
    - [IDMethodUsed]-vOTU-Database.fasta.fasta
    - A curated file of assembled viral sequences used as the reference database to calculate abundances for the above tables
    - [IDMethodUsed]-vOTU-Clusters.fna

    - A curated file of assembled viral sequences that represent the representative RNA viral sequences for each viral operational taxonomic unit

/Proteomics data:

- Raw files / predicted proteins: The raw DIA proteomic spectral data from each coral sample, ID within the file. Included are our DDA control samples, and our BSA control sample. Predicted peptides included in data.
- Transcriptomes: Built transcriptomes for analysis (Table 1 of proteome results)
- Viral peptides:
    - Predicted viral peptide sequences
    - BLASTP curated peptide database for identification
    - Viral_hits_high_confidence – Viral hits of high confidence, with E-values, bit scores, and sequences in supplementary files

4.3. Task 3 – Begin analysis of extracts from naive coral samples for metabolomic (SMS, GT).

Organic extracts obtained from diseased (*Colpophyllia natans*), healthy (*Orbicella faveolata*, *Montastraea cavernosa*), and exposed to disease (*Orbicella faveolata*, *Montastraea cavernosa*) coral fragments were analyzed via UHPLC-HRMS in both positive and negative ionization mode. Positive mode data were preprocessed with mzMine3 and the output was used to generate feature-based molecular networks (FBMN) to assist with unknown feature annotation. Additionally, positive mode data were also preprocessed with Thermo Scientific™ Compound Discoverer™ (ver. 3.3) software to generate a consolidated location for data analysis. Raw data files acquired in positive ionization mode were uploaded to the mass spectral repository MassIVE and are available at **https://massive.ucsd.edu** under the identifier MSV000094526.

Initial chemometric analysis was performed on all coral species included in this study to determine metabolome variation between species prior to further downstream statistical analysis. Principal component analysis was utilized to visualize the difference in metabolome between species and revealed differential clustering of each species. Therefore, to remove excess variation due to species, data acquired on *C. natans* and *O. faveolata* were not included in analysis between healthy controls and fragments exposed to disease. The diversity of metabolite features in healthy and disease exposed *M. cavernosa* fragments across all sampling periods was assessed and visualized in an alpha diversity plot (**Figure 3**). The alpha diversity for each sample was calculated by converting raw feature abundances to Bray-Curtis dissimilarity and Shannon index as the alpha diversity metric. While no statistical significance is captured between different time points of disease progression in either healthy or exposed to disease fragments, there is a trend in the exposed *M. cavernosa* fragments. The metabolite feature diversity decreases in the 48-hour post exposure sampling period (SP2) and gradually increases through disease progression. This trend is not captured in the control samples.

Figure 3. Alpha diversity plot of exposed to disease and control *M. cavernosa* (MCAV) fragments through different sampling periods (SP) of disease progression. Shannon entropy values were computed via qiime2 metabolomics plugin.

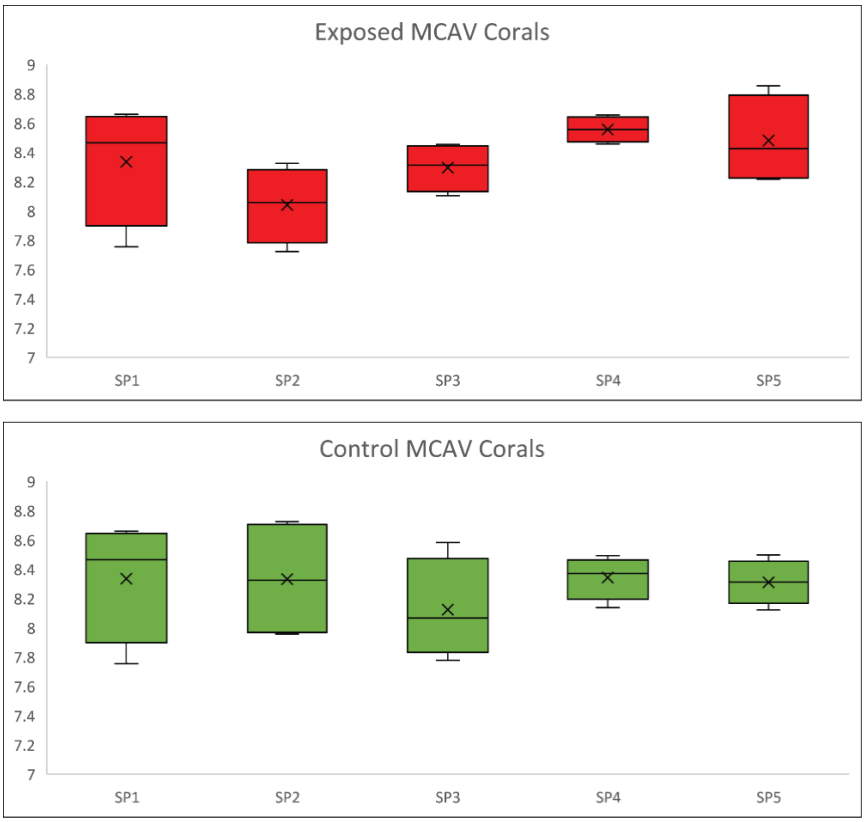

Principal component analysis (PCA) of healthy and exposed *M. cavernosa* fragments were constructed for each transmission time point to visualize the shift in metabolome through disease progression (**Figure 4**). Visually, the largest clustering of SCTLD exposed vs healthy fragments was captured at sampling period 2 or 48-hours after exposure, which suggests the largest metabolic response to SCTLD is observed prior to visual signs of infection. Furthermore, the metabolomes of healthy and SCTLD infected *M. cavernosa* display significant overlap at all later sampling periods. The differential clustering between healthy and SCTLD exposed groups was assessed via permutational multivariate analysis of variance (PERMANOVA) with all groups displaying significant overlap at all sampling periods but sampling period 2 (SP2, $p = 0.023$). Similarity percentage (SIMPER) analysis was performed using the Bray-Curtis transformed quantification matrix to determine the metabolite features responsible for driving differences between the healthy and SCTLD exposed groups at each sampling period. The identified metabolite features were compiled into a table (**SIMPER features_ED@All Time points.xlsx**) for each sampling period and annotation of these features were performed by spectral library matching through

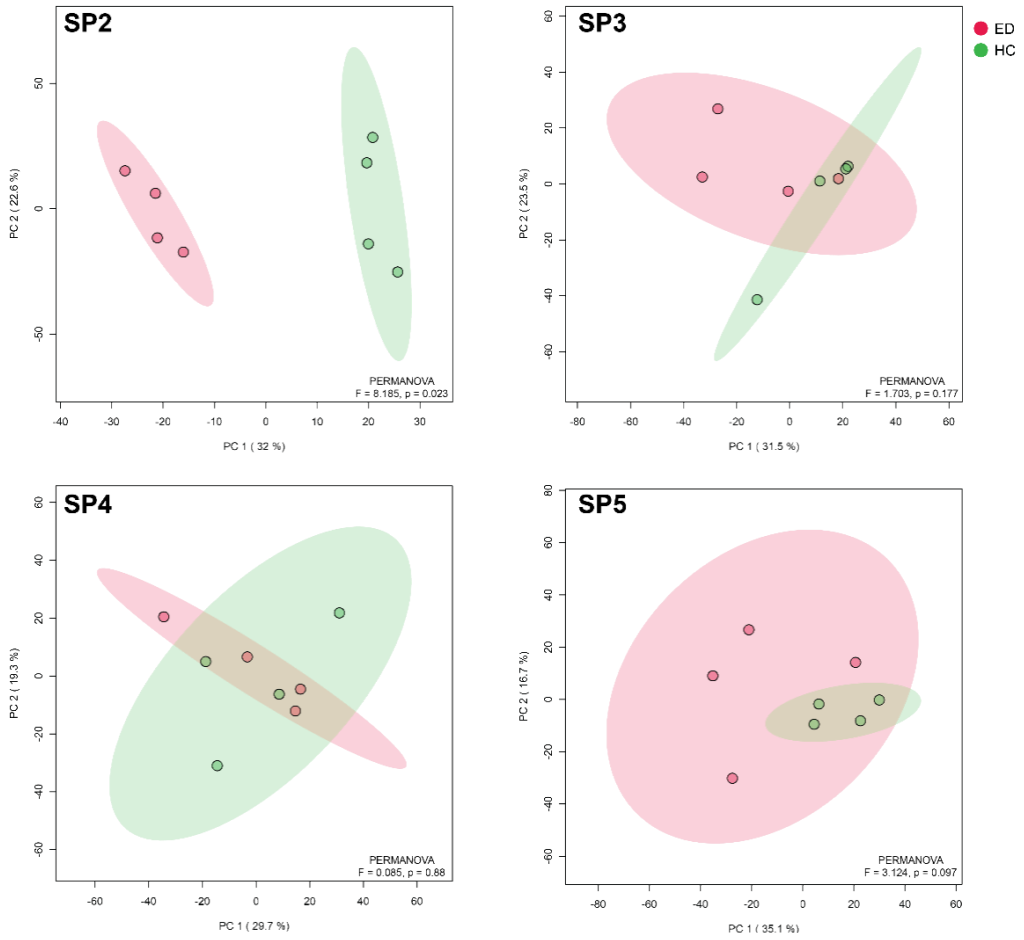

Figure 4. Principal component analysis of healthy (HC) and SCTLD exposed (ED) *M. cavernosa* fragments over different points of disease progression (SP2: 48-hours post exposure, SP3: first visual sign of infection, SP4: 7 days after SP3, SP5: 7 days after SP4). Plots were constructed via MetaboAnalyst 6.0.

Global Natural Products Social Molecular Networking (GNPS)[1] library matching and annotation propagation through feature-based molecular networking (FBMN) workflows. In instances where features received no spectral matches in databases and were not present in subnetworks containing spectral matches, annotation was performed via SIRIUS[2] an *in silico* fragmentation tool that provides class annotation of metabolite features based upon substructures identified in the fragmentation spectra.

The metabolite features driving differences between the healthy and SCTLD exposed *M. cavernosa* fragments were visualized in an UpSet plot to identify features unique and shared between each sampling period (**Figure 5**). Of the SIMPER identified features, 222 were detected across all sampling periods. Each sampling period contains unique metabolite features driving differences between healthy and SCTLD exposed fragments indicating that different features are implicated at disease onset and through disease progression. Among the metabolite features unique to each group, 57 were detected in 48-hours post exposure (SP2), 13 were detected exclusively at first visual signs of disease (SP3), 24 were detected in the 7-day post visual disease (SP4), and 56

were detected in the final disease sampling period (SP5). The 48-hour post exposure time point (SP2) contains the largest number of unique intersections followed closely by the final visual disease sampling period (SP5). The largest number of unique features being detected pre-visual signs of disease suggests that the metabolome of the holobiont shifts rapidly in response to SCTLD infection despite the absence of lesions on the infected colony. Furthermore, the second largest number of unique metabolite features are contained in the final sampling period, SP5, which could indicate that unique compounds are involved in late disease stages rather than consistent through visual disease stages.

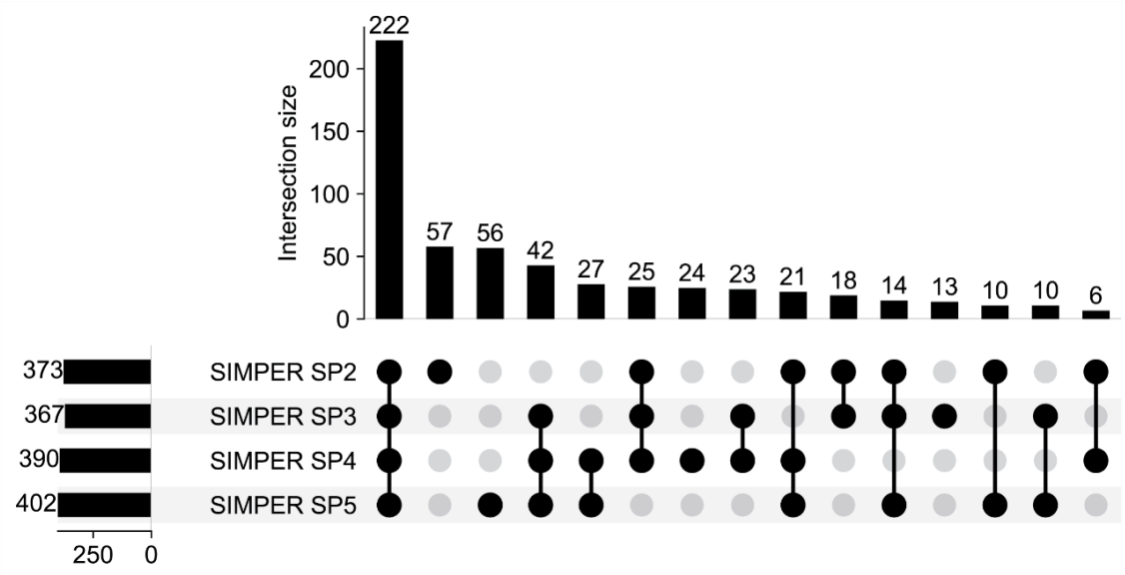

Figure 5. UpSet plot of metabolite features determined to be driving differences between healthy and SCTLD exposed *M. cavernosa* fragments via SIMPER analysis (SP2: 48-hours post exposure, SP3: first visual sign of infection, SP4: 7 days after SP3, SP5: 7 days after SP4). Plot construction was performed using Jupyter Notebook.

Annotation of SIMPER identified features was attempted through spectral library matching, FBMN and in cases where structures could not be proposed class annotations were provided through SIRIUS for all compounds with the ClassyFire score greater than 0.8. All metabolite features with a ClassyFire score greater that 0.8 identified by SIMPER at SP2 were visualized in a sunburst plot to guide annotation of features within a class and subclass (**Figure 6**). Of the annotated features, several were detected across all healthy vs SCTLD exposed defined SIMPER groupings including acylcarnitines (CAR), diacylglyceryl-carboxyhydroxymethylcholine (DGCC), and lyso-platelet-activating factors (lyso-PAF) indicating that the abundance of these lipids are changing not only in response to the infectious agent for SCTLD but also as the disease progresses. Lyso-PAF is a precursor to PAF which is a bioactive lipid involved in inflammation[3]. These compounds have been previously detected in scleractinian coral tissue and have been shown to be involved in non-self interaction with algal, fungal, and coral species[4] as well as various *Vibrio* species[5]. Additionally, lyso-PAF and PAF have been detected in higher abundance in growing regions of coral tissue and in coral tissue exposed to excess UV radiation[6]. The identification of lyso-PAF as a driver of differences between healthy and SCTLD exposed fragments via SIMPER suggests that these lipid mediators of inflammation are involved in immune response to SCTLD infection. Additionally, lyso-PAF were identified as drivers of differences by SIMPER at each

(MGDG) and digalactosyl-diacylglycerols (DGDG). These lipids are an integral component of the thylakoid membrane of endosymbiotic algae and changes in composition have been reported in corals exposed to temperatures that induce bleaching[10]. These compounds are detected in differential abundance between healthy and SCTLD exposed fragments which could indicate breakdown in photosynthetic apparatus during SCTLD infection.

Extract used for the metabolomics analysis were also processed for antibacterial assays. Progress for this process is described in file ##########.

4.4. Task 4 – Process naïve coral samples for histology and digitizing histological slides (FWC, GMU).

Gross observations

Tissue Loss

The number of DD and ED specimens showing tissue loss (Figure 7) was reported to DEP in Year 1 (Ushijima et al. DEP final report 2024); however, individual specimens with this condition are now listed in Table 4. No HC specimens had tissue-loss lesions.

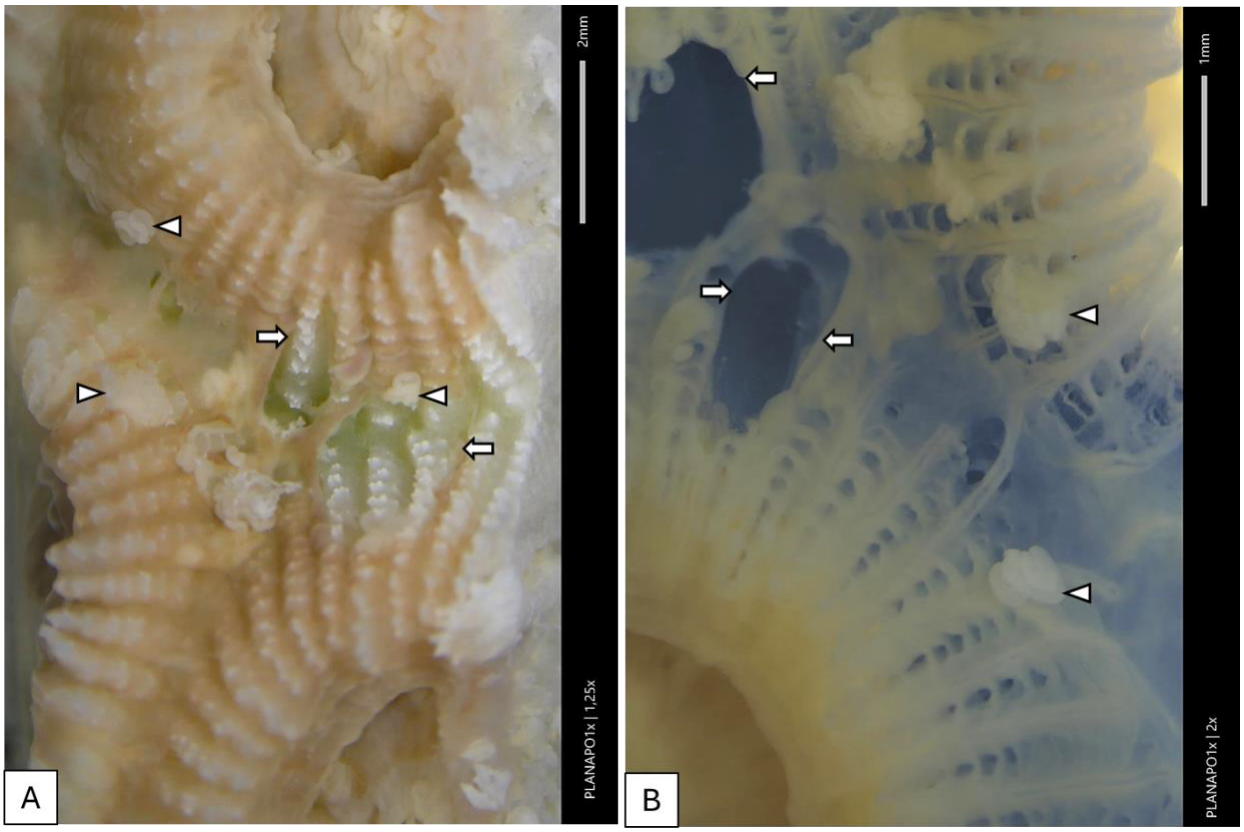

Figure 7. MCAV_1081_0523TS146, recipient apparently healthy coral sample collected 8d after first exposed to disease (ED). (A) External oral surface view of fixed tissue before decalcification; arrowheads indicate protrusion of mesenterial filaments and arrows indicate the tissue-loss areas. (B) External oral

surface view of the same area as (A) after decalcification. Note the lysed-like appearance of the coenenchyme at the tissue-loss areas (arrows) and the protruded mesenterial filaments (arrowheads).

Protruded mesenterial filaments

The number of DD and ED specimens with protruded mesenterial filaments (Figure 7) was also reported to the DEP in Year 1 (Ushijima et al. DEP final report 2024); however, individual specimens with this condition are now listed in Table 4. No HC specimens had protruded mesenterial filaments.

Histology

Experimental Groups

Descriptions of the primary microscopic lesions present in the tissues of these groups are presented in this section and the percentage of fragments affected by each condition are shown in Table 5. Other observations of note were endolithic suspect fungal hyphae that were infecting deep basal body wall coral cells in the samples that were in the worst condition, crystalline inclusion bodies (CIBs; Landsberg et al. 2020) detected regardless of health conditions in two genotypes of MCAV: McH-103 (4) red (N = 9; i.e., all tested HC and ED) and McH-101 white (N = 5; 3 ED, and 2 HC), and ciliates that were sporadically detected in healthy baseline control (HH) MCAV (N = 1), healthy control (HC) OFAV (N = 1), disease donor CNAT (N = 2), and disease donor OFAV (N = 1). *Trichodina* (another ciliate species) were detected in disease donor CNAT (N = 5). Because these were not considered to be affecting the health of the fragments, they will not be discussed further.

Table 5. Combined number (N) examined and prevalence (parenthesis) for sample health indicators: gross observations of tissue loss (TL) and protruded mesenterial filaments (MFP), and histological observations of endosymbiont necrosis (ZXNEC), absence of endosymbiont starches (PAS-), degraded granular amoebocytes (globules, GLB), suspect and apparent lytic necrosis (LN), and suspect and apparent stony coral tissue loss disease (SCTLD). Species include Colpophyllia natans (CNAT), Montastraea cavernosa (MCAV), and Orbicella faveolata (OFAV). Sample health codes include diseased donor corals from the field (DD), pre-experiment naïve apparently healthy corals (HH), apparently healthy corals exposed to healthy corals (HC), and apparently healthy corals exposed to diseased donor corals (ED).

Species Health code (N) examined	**CNAT DD 8**	**MCAV DD 1**	**OFAV DD 2**	**MCAV HH 4**	**MCAV HC 20**	**MCAV ED 16**	**OFAV HH 1**	**OFAV HC 5**	**OFAV ED 4**	**All Total 61**
TL	7 (88%)	1 (100%)	2 (100%)	0 (0%)	0 (0%)	7 (44%)	0 (0%)	0 (0%)	1 (25%)	18 (30%)
MFP	1 (13%)	0 (0%)	0 (0%)	0 (0%)	0 (0%)	6 (38%)	0 (0%)	0 (0%)	0 (0%)	7 (11%)
ZXNEC	8 (100%)	1 (100%)	2 (100%)	1 (25%)	18 (90%)	15 (94%)	1 (100%)	5 (100%)	4 (100%)	55 (90%)
PAS-	7* (100%)	1 (100%)	2 (100%)	0* (0%)	1 (5%)	10** (71%)	0 (0%)	0 (0%)	3 (75%)	24*** (42%)
GLB	8 (100%)	0 (0%)	2 (100%)	0 (0%)	3 (15%)	13 (81%)	0 (0%)	0 (0%)	0 (0%)	26 (43%)
Suspect LN	0 (0%)	0 (0%)	0 (0%)	0 (0%)	9 (45%)	10 (63%)	1 (100%)	4 (80%)	1 (25%)	25 (41%)
LN	8 (100%)	1 (100%)	2 (100%)	0 (0%)	0 (0%)	3 (19%)	0 (0%)	0 (0%)	3 (75%)	17 (28%)
Suspect SCTLD	0 (0%)	0 (0%)	0 (0%)	0 (0%)	0 (0%)	10 (63%)	0 (0%)	0 (0%)	1 (25%)	11 (18%)
SCTLD	8 (100%)	1 (100%)	2 (100%)	0 (0%)	0 (0%)	3 (19%)	0 (0%)	0 (0%)	3 (75%)	17 (28%)

*Indicates one sample in the group was not able to be assessed; percentage based on those assessed.
**Indicates two samples in the group were not able to be assessed; percentage based on those assessed.
***Indicates four total samples were not able to be assessed; percentage based on those assessed.

We also examined the Giemsa-stained histoslides to learn more about the location and morphology of suspect gram-negative or other types of bacteria that might be in the coral tissues, particularly focusing on magenta-colored coccobacilli (MCBs) that had been found during the original histological examination of apparently healthy and SCTLD-affected corals collected from the Florida Keys (Landsberg et al., 2020; Hawthorn et al., 2023). This task was started after reading the H&E, thionin, and PAS-MY histoslides by YK and LH; however, not all Giemsa slides at FWRI have been read, and EP has not yet read the GMU Giemsa slides because that set was sent to iHisto for scanning. Without observer consensus resolved, Giemsa data are not included in this report. Reading and interpretation of these histoslides will continue. As was originally noted by Jan Landsberg (personal communication, 2019), granular vesicles containing mucus in early stage mucocytes will stain with Giemsa and we need to look for uniform sizing and shape of the magenta-stained granules to be sure they are suspect MCBs.

Disease Donor (DD)

Disease donor colonies were prepared from three species (CNAT, MCAV, and OFAV). However, one of the two OFAV colonies was not OFAV (1111-296, OfD-40), based on the lack of acidophilic granular amoebocytes in the mesenteries of the oral region of the polyps that are found in OFAV and *Orbicella annularis* (OANN), and having large granular amoebocytes interspersed between mucocytes and gastrodermal cells in the lower mesenteries and cnidoglandular bands containing granules that were staining pale purple (basophilic). This colony might be *O. franksi* (OFRA), which may contribute to

different results when comparing microbiome and molecular results. For consistency in this report, however, this colony is still referred to as OFAV.

All DD colonies were confirmed as showing tissue changes consistent with SCTLD, including lytic necrosis, zooxanthellae necrosis, and globule formation from degrading granular amoebocytes. Increased numbers of large mucocytes were present in the internal oral and aboral regions of the mesenteries. Staining of the mucus with the thionin procedure provided information on its relative consistency in different areas of the polyps, and paler staining was observed in the deep gastrovascular cavities and as mucus released by lysing of the mucocytes became diluted with seawater along the epidermis. The more severely necrotic and fragmented polyps' basal body walls showed infiltration of mucus as the membranes of the lipid vesicles lysed. These lesions will be discussed further in Results below.

Controls (HH and HC)
Coral fragments prepared from the available naïve colonies were identified as four different genotypes of MCAV, color labeled as blue McH-102(1), orange McH-104, white McH-101, and red McH-103(4), and one colony of OFAV, yellow OfH-106. These fragments were placed in separate tanks by genotype and whether they would be exposed to DD colonies or Controls. At the start of the experiment (0d), one fragment of each genotype was sampled to understand the baseline condition of the fragments (HH). Of the MCAV HH samples, one (1052-001), and the OFAV sample (1056-021), were in fair and poor condition, respectively. They had necrotic zooxanthellae, atrophied epidermis, and detached gastrodermis on the surface body wall, which was more developed in the OFAV sample, with mucocytes lysing and filling in the area next to the mesoglea with mucus as occurred in lytic necrosis.

Control fragments were sampled at specified intervals (see Table 4) from 2d to 41d after the start of the experiment. As early as 2d after the start, the control tissues never did resemble what would be expected of fresh, field-collected specimens and their abnormal appearance, with areas of wide space between the surface body wall and detached gastrodermal cells, as well as hypertrophied mucocytes and necrotic endosymbionts resembling lytic necrosis, in these corals made it difficult to determine what was happening to the control fragments. MCAV (1096-221) and OFAV (1097-226) sampled 36d after the start of the experiment, and OFAV (1102-251) sampled at 41d, had severe epithelial necrosis and tissue fragmentation, loss of cells from the epidermis with marked basal vacuolation and karyorrhectic debris, as well as sloughed epidermis over septa; necrosis and loss of endosymbionts; hypertrophied mucocyte development and lysing in oral mesenteries and gastrodermis; basal tentacle epidermal necrosis, and masses of necrotic gastrodermal cells filling gastrovascular canals along the coenenchyme. The severity of the pathological tissue changes was in many ways consistent with SCTLD lesions.

Exposed to SCTLD (ED)
Among the same genotype fragments in the separate tanks exposed to DD colonies, definite lesions meeting the criteria for SCTLD were identified as early as 2d following

the start of the exposure (Table 4). However, not all fragments in the tanks were found to have SCTLD. For example, for Time Point 4, this condition was not confirmed in MCAV (blue, orange, and white genotypes) collected 10–12 days after the experiment started in Table 1, while samples collected before or after this date were diagnosed with SCTLD or suspect SCTLD. On the other hand, at this Time Point 4, grossly visible tissue loss along with protruded mesenterial filaments were detected in two sampled specimens (blue and red genotypes). The samples were also associated with the emergence of degraded granular amoebocytes in the mesenterial filaments (see below).

Health Indicators

The following histological tissue health indicators were reviewed and tabulated for all samples (Tables 4 and 5), to assess the condition of the sample and the SCTLD diagnosis.

Endosymbiont (Zooxanthellae) Necrosis

Deformed shape and/or loss of nuclear and cytoplasmic details of endosymbionts.

Endosymbiont Starch Granules

Slides stained with PAS-MY were examined for the PAS reaction of the endosymbionts' starch granules. Positively stained starch granules (PAS+) indicated endosymbionts were storing starch (carbohydrates) produced during photosynthesis; decreasing amounts of (PAS+) staining of starch granules indicated declining condition of endosymbionts, with no staining (PAS-) an indicator of poor endosymbiont condition (Tables 4 and 5). In the experiment, the overall PAS results were as follows: moderately to lightly positive in HH and HC, lightly positive to negative in ED, and negative in DD (Figure 8).

Degraded Granular Amoebocytes (Globules)

We identified hyaline globules (or droplets) as the final stage of degraded granular amoebocytes (Figure 8) located in the mesenterial filament lobes adjacent to the cnidoglandular band in some disease-exposed (ED) MCAV specimens, as well as in disease donor (DD) specimens, including CNAT and OFAV species (Table 4). Globules (diameter of ca. 10 μm at maximum) were mostly eosinophilic, but sometimes included light greyish stain, with a distinct outer ring stained slightly darker. Occasionally globules were found with peripherally located pale swollen nuclei and the degraded cytoplasm sometimes stained homogeneously brown-green-orange (with eosin). Necrosis of the mesenterial filaments' epithelium was also observed (Figure 8A). Among the tested MCAV specimens, these degraded granular amoebocytes were most frequently observed in ED (13/16); however, they were also lightly present in some HC samples (3/20; Table 1).

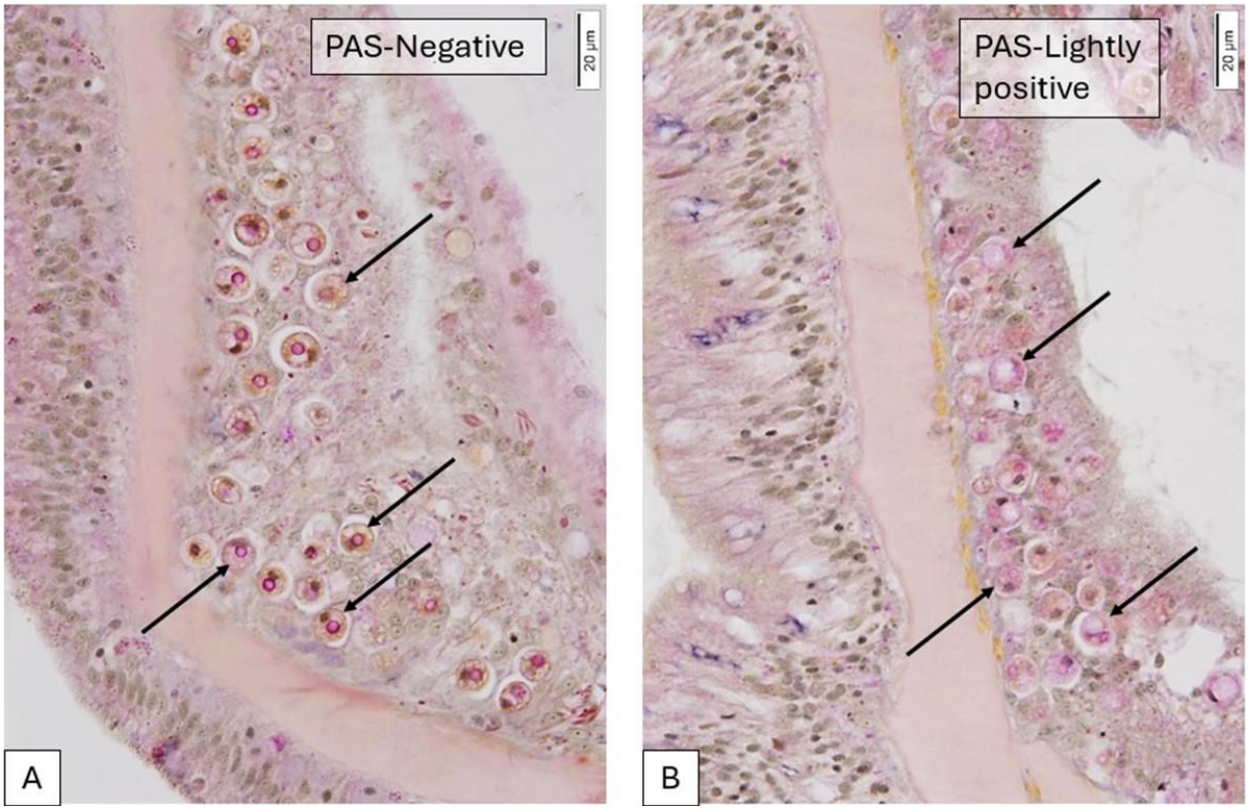

Figure 8. Histological section of MCAV surface body wall, showing the gastrodermis with endosymbionts' periodic acid-Schiff's reagent (PAS) stain reaction. (A) PAS negative (arrows) in ED (8 d post-exposed; MCAV_1081_146_ED). (B) PAS lightly positive (arrows) in HC (10 d control; MCAV1083_156_HC). PAS-MY stain.

Lytic Necrosis

Apparent or suspected lytic necrosis of the gastrodermis (marked as LN*) was observed in ED and DD specimens for the tested species (Table 4, Figure). However, we also found pathological changes that would support their interpretation as lytic necrosis in deteriorated tissues of HC samples for both MCAV and OFAV (Table 4). In addition to necrotic zooxanthellae that might be in enlarged symbiosomes, atrophied epidermis, increased hypertrophied mucocytes in the gastrodermis of the surface body wall with apical vacuoles in the non-mucocyte cells, the gastrodermis separated partially from the mesoglea as well; this space might be filled with mucus or fluid in the thionin-stained slides. Since it was not completely detached or sloughing into the gastrovascular cavities and canals and the epidermis remained firmly attached to the mesoglea in most areas, we decided that these samples should be interpreted as "Suspect." The issue with the control group is discussed further in the Discussion.

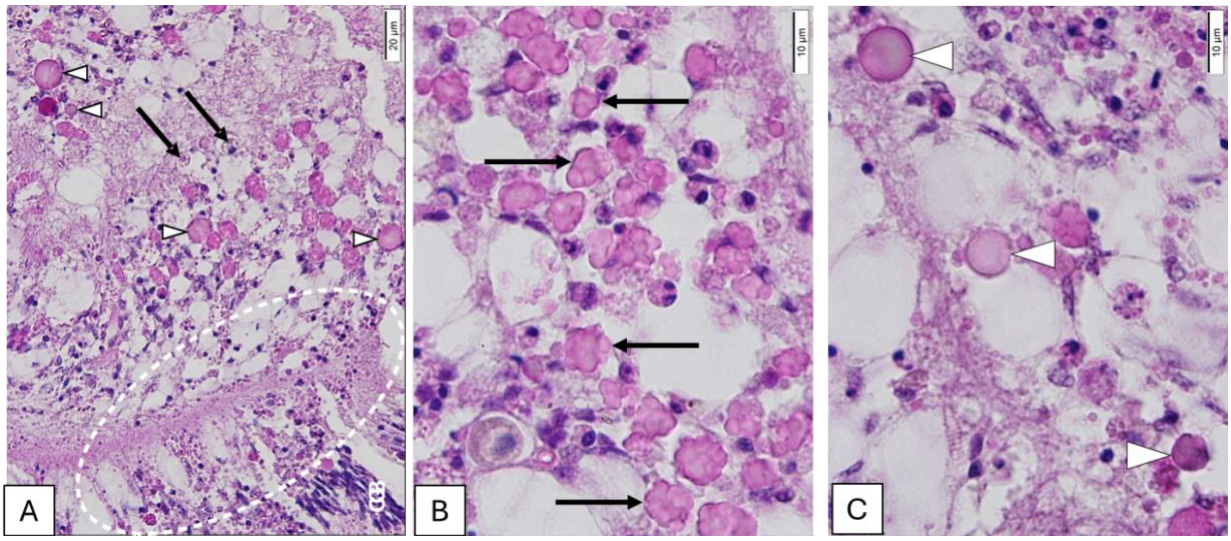

Figure 9. Histological section of mesenterial filament of MCAV_1081_0523TS146, stained with hematoxylin and eosin (H&E). The recipient apparently healthy coral sample was collected 8 days after exposure to diseased coral (ED). (A) Abundant globules (arrowheads) are degrading amoebocytes found in vacuolated and necrotic gastrodermal cells of lobes adjacent to the necrotic filament (nuclear karyorrhexis, dotted circle). Arrows indicate degenerated/necrotic endosymbionts. CGB = cnidoglandular band. (B) Granular amoebocytes started to round up and aggregated, presume transitional stage to globular form. (C) High magnification of (A) with degraded amoebocytes (arrowheads).

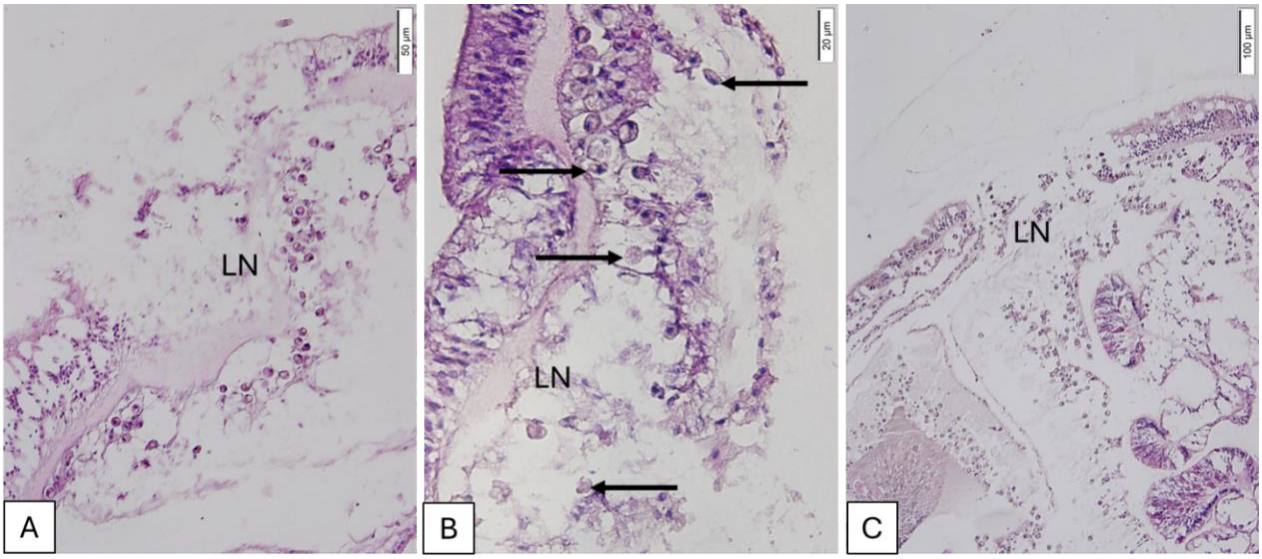

Figure 10. Histological section of coral tissues showing gastrodermis with lytic necrosis (LN) lesions (H&E). (A) SCTLD disease donor CNAT (1057_026). (B) Disease-exposed naïve MCAV specimen (1067_076) with necrotic, deformed shape endosymbionts (arrows).(C) Disease-exposed naïve OFAV specimen (1071_069).

SCTLD Diagnosis

All donor corals including CNAT, MCAV, and OFAV were diagnosed as SCTLD positive based on histopathological examination and findings of multiple pathological changes described in Landsberg et al. (2020) and Hawthorn et al. (2023). SCTLD-positive cases were found in naïve MCAV (3/16) and OFAV (3/4) that were induced with

the disease donor (Tables 1 and 2), beginning as early as 2d following the start of the experiment. Suspected SCTLD-positive cases were observed in naïve MCAV (10/16) and OFAV (1/4) that were induced with the disease donor (Tables 4 and 5); they did not meet all the criteria for SCTLD (e.g., lacking definitive lytic necrosis of the gastrodermis) when compared with the SCTLD-positive donor samples.

Histoslide Digital Scanning
The scanning request for iHisto included these special stains (numbers of histoslides indicated in parentheses): H&E (N = 60), thionin (N = 60), Giemsa (N = 60), and PAS-MY JB4 (N = 57) sections. All of the resulting digitized files were uploaded to FWRI's eSlide Manager system network.

4.5. Task 5 – Embed any remaining naïve corals for TEM and image 15 more corals (UNCW) as well as analyze 10 already-imaged corals (UNCW & UPR).

The TEM portion of this report included three separate projects: the SCTLD Holistic Time Series, the time series from the Dry Tortugas, and a potentially new *O. faveolata* coral disease. A breakdown of the number of samples, micrographs, and symbionts scored for each project is provided in Table x. For the rest of the report, the results and discussion will be broken into separate sections based on the project.

Table 6. A summary of the number of coral samples imaged and symbionts scored for the 24-25 fiscal year.

	Time Series	**Dry Tortugas**	**Acute Orbicella**	**Total**
Coral Samples	15	10	5	30
Total Micrographs	1090	372	483	1945
Total Symbionts Scored	160	106	209	475

Though there were more symbionts scored, only 122 included were in these analyses as they created a complete set of experimental and control corals. Samples included three health states: naïve (HH), exposed to disease (ED), and healthy controls (HC) and five different time points with the symbionts scored listed within Figure 11.

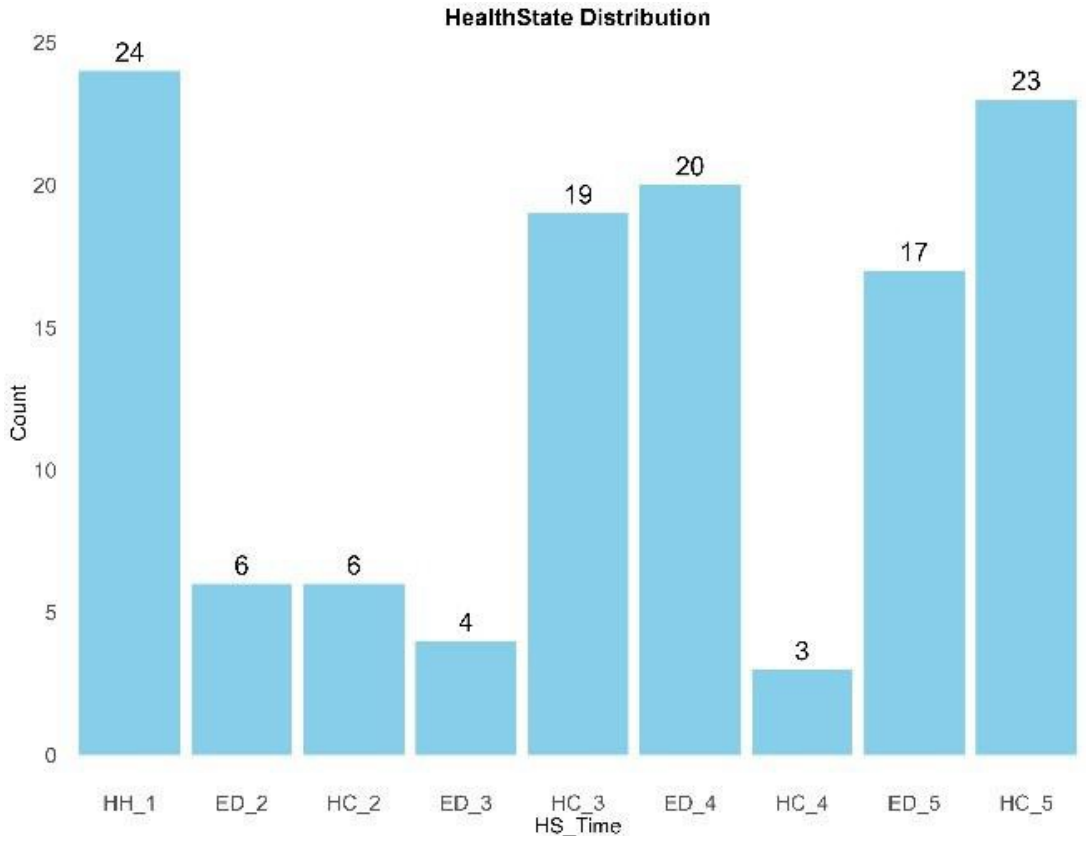

Figure 11. A bar graph showing the number of symbionts scored by health state and time point.

Symbiont cell size was significant among the different groups ($p = 0.0088$), those from ED at T2 being larger than those at T3 ($p = 0.0424$) and T4 ($p = 0.0369$) (Fig 12). Additionally, symbionts from HC at T2 were also larger than those at T3 ($p = 0.0248$) and T4 ($p = 0.0320$). These findings particularly at T2 could be due to the low sample size for ED and HC health states – further sampling is necessary to better analyze these differences.

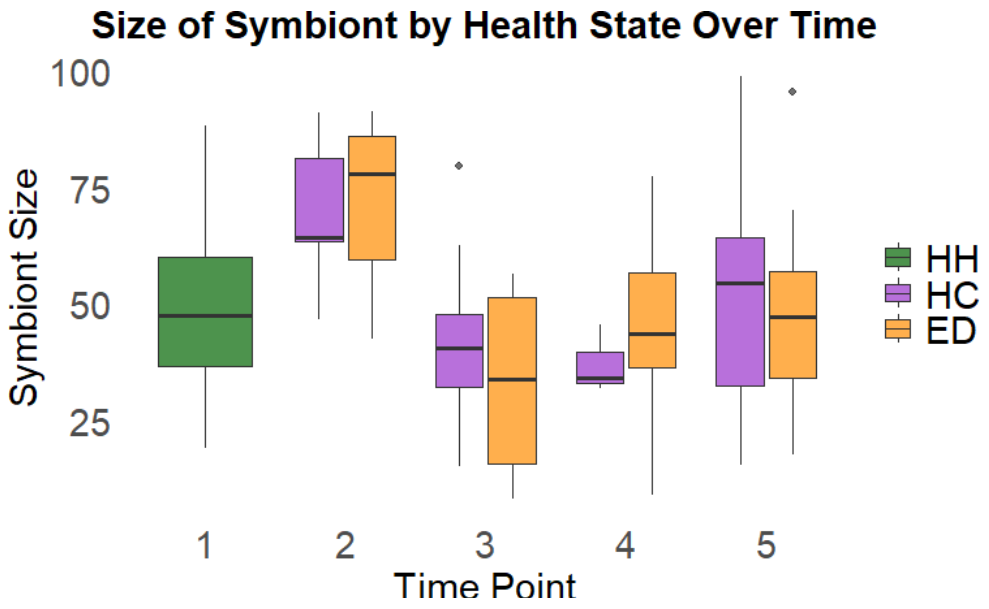

Figure 12. A boxplot showing the size of the symbiont by health state over time.

Starch number was also significant among the dataset (p = 2.91e-13). ED at T2 had more starches than those at T3 (p = 0.0311), T4 (p = 0.0041), and T5 (p = 0.0061). This could be an indication of building starch reserves during the initial exposure to SCTLD or it could be due to the smaller sample size at this time point. Symbionts from ED corals contained less starch than those from HC corals at T3 (p = 0.0158), T4 (p = 0.0144), and T5 (p = 0.0000). Additionally, ED corals contained symbionts with larger starches than HC at T3 (p = 0.0128), T4 (p = 0.0062) and T5 (p = 0.0000). Lastly, naïve corals (HH) contained more starches and larger starches than ED corals at T3 (p = 0.0017; p = 0.0016), T4 (p = 0.0000; p = 0.0000), and T5 (p = 0.0000; p = 0.0000). Starch size (p = 4.244e-13) was also significant. When looking at ED corals over time, symbionts at T2 has significantly larger starches than T3 (p = 0.0207) and T4 (p = 0.0022). The trends show that starches decline in number and in size in the symbionts in the exposed to disease corals, mimicking a similar trend seen in the SCTLD field time series from the Dry Tortugas (Fig 13).

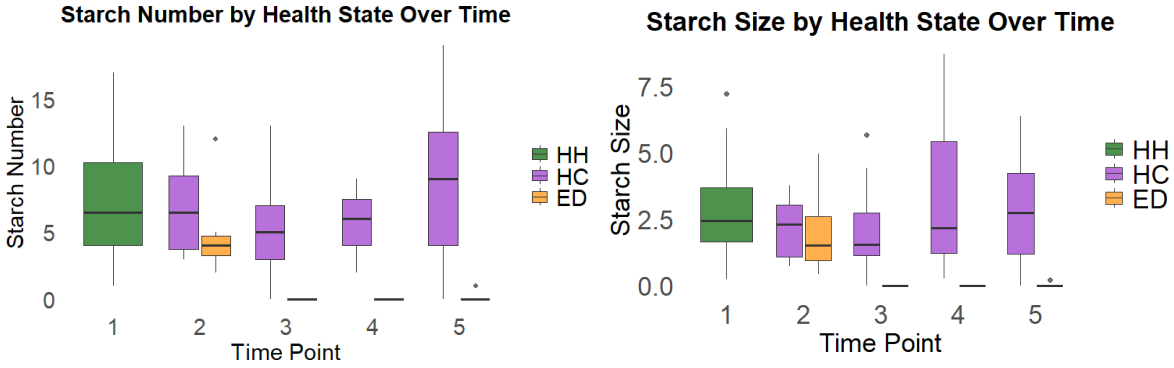

Figure 13. A boxplot showing the number (left) and size (right) of starches over time by health state.

Lipid number was also an important factor (p = 3.09e-10), with symbionts from ED corals at T2 containing more than those at T4 (p = 0.0034) and T5 (p = 0.0014). Moreover, at T5 symbionts from HC corals had more than those from ED (p = 0.0001). Naïve corals had substantially more lipids than ED (p = 0.0197) and HC (p = 0.0206) symbionts at T3, as well as ED corals from T4 (p = 0.0000) and T5 (p = 0.0000). The lipid size was also significant (p = 4.274e-10), and symbionts from ED corals at T2 had larger lipids than those from T4 (p = 0.0025) and T5 (p = 0. 0006). Though a larger sample size is needed, the trends indicate that lipid reserve decrease over time and this is more drastic for the exposed to disease corals (Fig 14).

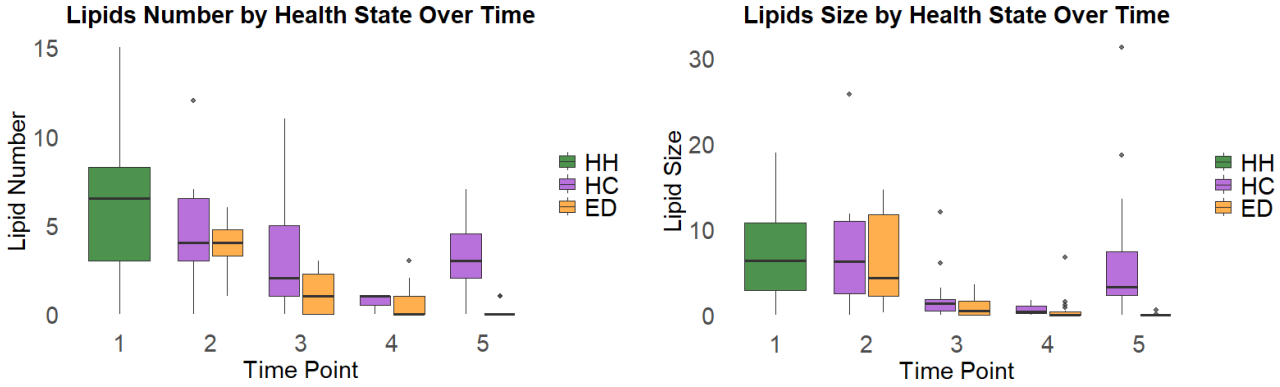

Figure 14. A boxplot showing the number of lipids by health state over time (left) and the size of the lipid droplets by health state over time (right).

The crystal presence (p = 2.684e-12) and area (p = 4.028e-12) were significant for this dataset. ED at T4 and T5 are the only groups with crystals, so all pairwise comparisons are significant when compared to that health states at those time points (Fig 15). It is interesting to note the presence and size of these crystal increases over time and is only present in the diseased samples, potentially indicating a correlation between this ultrastructure and disease.

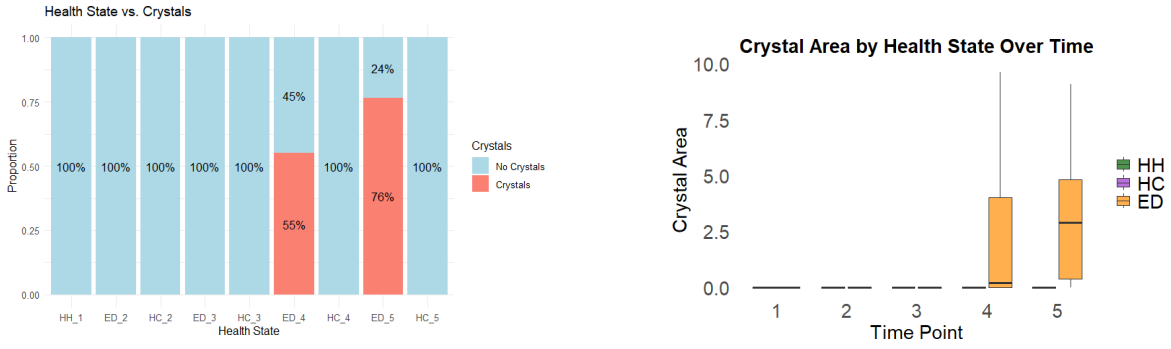

Figure 15. A proportion graph of the presence of crystals (left) and the area of the crystals (right) over time for each health state.

The presence of VLPs was statistically significant across the dataset ($p = 0.000254$) with pairwise significance among symbionts from HH at T1 and ED at T2 ($p = 0.000319$), ED at T4 ($p = 0.0232$), and ED at T5 ($p = 0.019$) (Fig 16). It is interesting to note that the naïve corals (HH) were not significantly different from the healthy control (HC) corals at any time point and the HC corals did not significantly differ from the ED corals at any time point. Though the trend seems to indicate that VLPs maybe be related to disease, when the controls are compared to the diseased experimental corals, there is no difference in VLP presence. The presence of the VLPs may have increased in the experimental samples compared to the initial naïve sample due to environmental changes, feedings, or other factors. More research needs to be done to further understand if there is a link between VLPs and SCTLD.

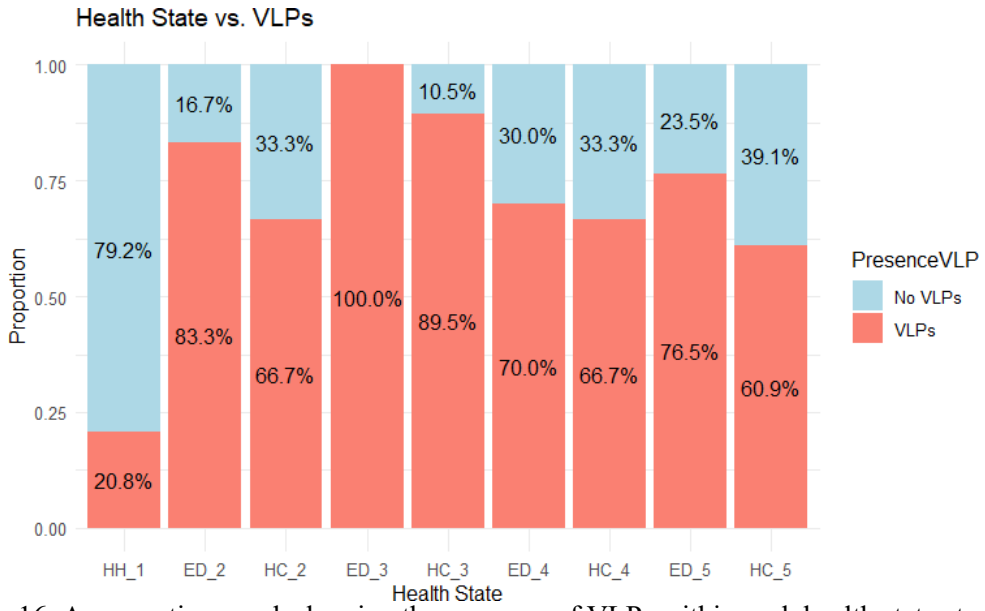

Figure 16. A proportion graph showing the presence of VLPs within each health state at each timepoint.

Some of the numerical variables were plotted on an NMDS plot by health state and time point. The trend indicates that the health states become more tightly clustered over time, and they become more distinct over time (Fig. 17).

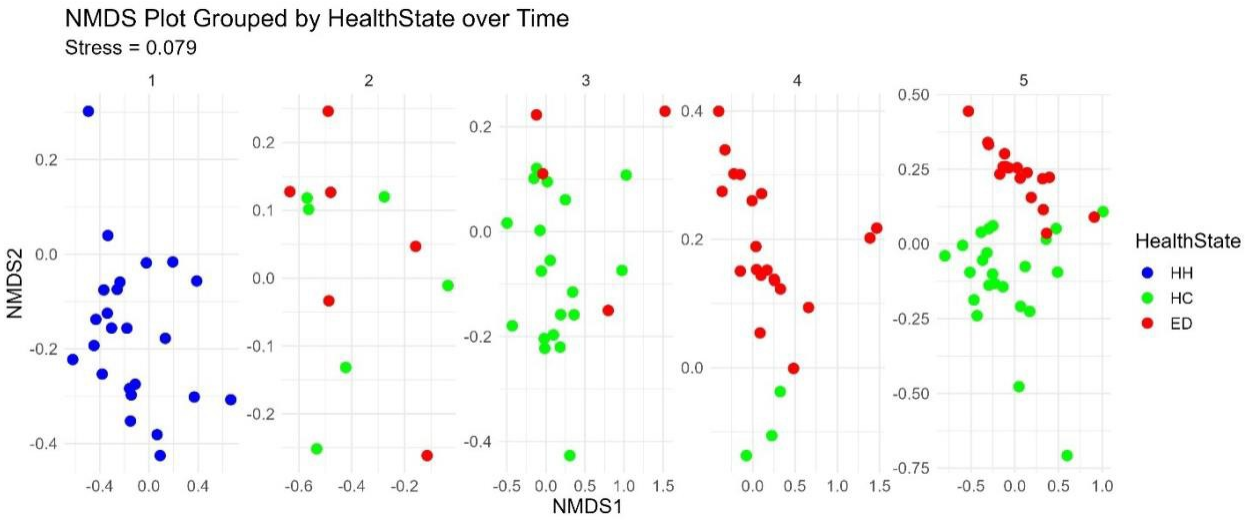

Figure 17. An NMDS incorporating symbiont area, starch size, crystal area, lipid size, number of lipids, and number of starches separated by time point.

Though the presence of electron dense bodies was also statistically significant across the dataset (Chi p = 0.000756), there are no significant pairwise differences between health state and time points. Cavity presence and size, broken down, symmetrical, pyrenoid, starch around pyrenoid, thylakoid breakdown, chloroplast breakdown, separation from cell wall, separation from symbiosome, and accumulation bodies were not significant between health states or time points.

4.6. Task 6 – Begin microbiome analysis of infected and control naive corals (UF).

Characterization of coral microbiomes through 16S rRNA amplicon libraries

The V4 hypervariable region of the 16S ribosomal RNA genes was successfully sequenced for all 61 coral microbiome samples, including naive healthy corals sampled pre-experiment only, diseased donor corals sampled pre-experiment and at the final timepoint, and experimental *Montastraea cavernosa* or *Orbicella faveolata* corals exposed to either a healthy or disease donor coral and sampled at five timepoints. Due to the lack of replication with the *O. faveolata* coral, those samples were removed in some downstream analyses. All raw sequencing reads are publicly available in NCBI under BioProject PRJNA1120034 (https://www.ncbi.nlm.nih.gov/bioproject/1120034). A total of 2,917,578 sequencing reads passed QC, with an average of 47,829 reads per sample. A total of 12,418 ASVs were identified from the full dataset of 61 samples. After filtering low abundance taxa and removing *O. faveolata* samples from the analysis, the final dataset included 1,018 ASVs across 49 coral microbiome samples.

Beta diversity of coral microbiome samples

Overall, microbiome composition varied by health state ($R^2 = 0.14$, $p < 0.001$) and timepoint ($R^2 = 0.12$, $p = 0.004$) (Figure 18). Post-hoc analysis did not detect significant differences in pairwise comparisons between timepoints (adjusted $p > 0.05$). Within

experimental treatments, microbiome composition did not change over time in either corals exposed to disease (ED) or healthy control corals (HC) ($p > 0.05$). In contrast, the microbiomes of disease donor corals (DD) differed between timepoints 1 and 5 ($R^2 = 0.18$, $p = 0.014$). In addition, microbiomes became more variable over time, regardless of health state ($p = 0.007$) (Figure 19).

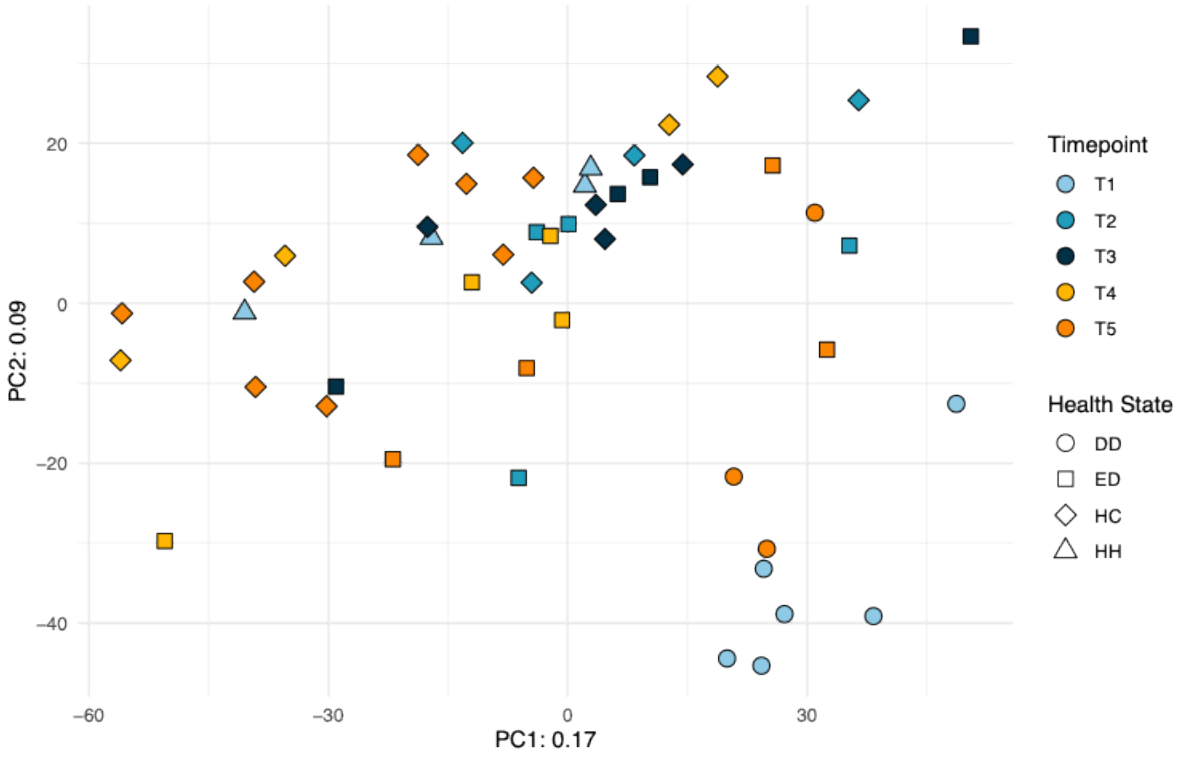

Figure 18. Ordination of the principal components analysis of 49 coral microbiome samples during the experimental transmission of stony coral tissue loss disease. Principal components 1 and 2 explained a total of 26% of the variation in coral microbiome composition. Points are colored by timepoint during the experimental transmission study. The shapes of points indicate the coral health state where DD represents disease donor corals used to transmit disease, ED represents experimental corals exposed to disease, HC represents experimental corals exposed to healthy corals, and HH represents healthy naive corals before experimental exposures.

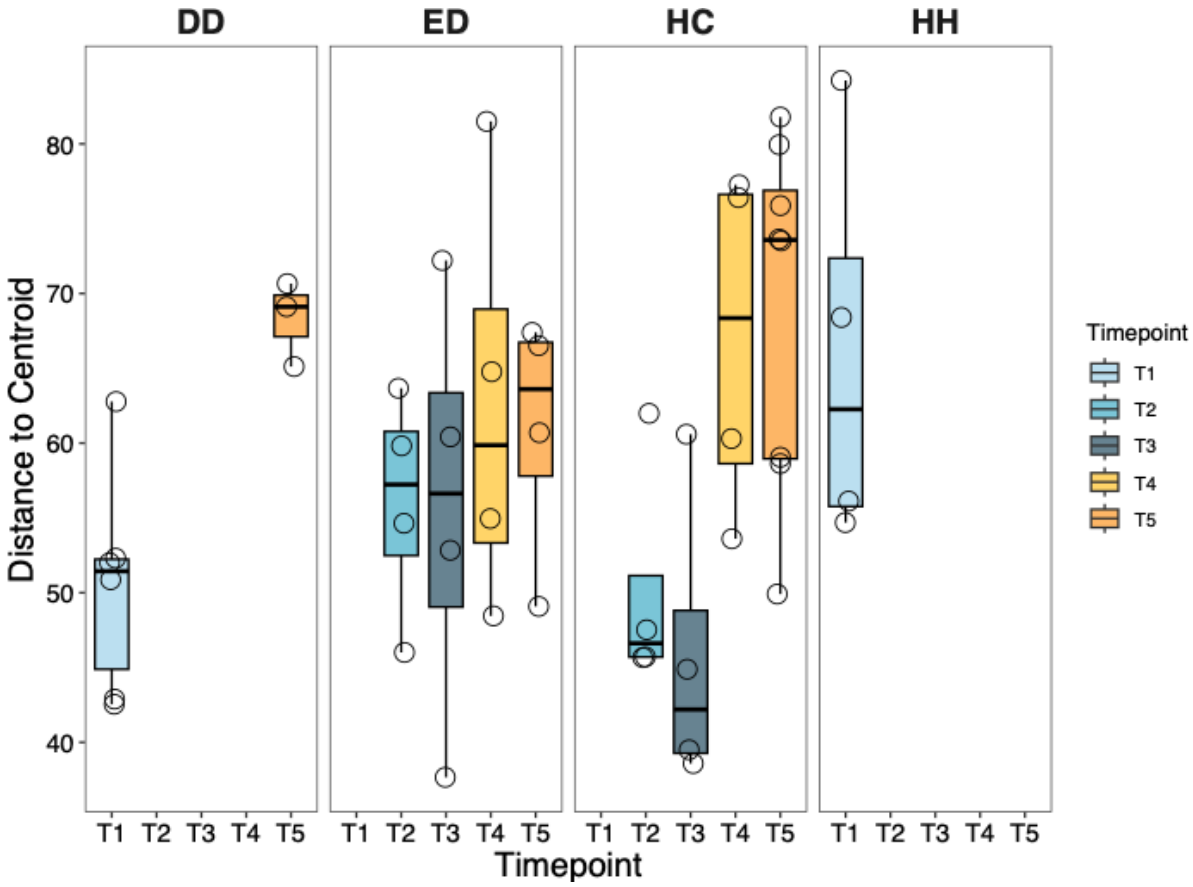

Figure 19. Dispersion of beta diversity, calculated as distance to centroid, within each health state across time. Increased distance to centroid indicates a more variable microbial community composition. Boxes are colored by timepoint during the experimental transmission study. Plots are faceted by the coral health state where DD represents disease donor corals used to transmit disease, ED represents experimental corals exposed to disease, HC represents experimental corals exposed to healthy corals, and HH represents healthy naive corals before experimental exposures.

Differentially abundant taxa in disease-exposed corals

To determine what taxa were changing over time in the disease-exposed colonies, we identified amplicon sequence variants (ASVs), representative of bacterial strains, that were present in disease-exposed colonies but not in healthy-exposed colonies. We detected a total of 234 ASVs were enriched in the disease-exposed corals. These ASVs were compared to ASVs previously associated with SCTLD in the Rosales et al. (2023) meta-analysis.

We identified 21 sequence variants that changed in disease-exposed colonies at each timepoint and that were identical to sequences previously associated with SCTLD. Successional patterns were observed among these SCTLD-enriched taxa, as most taxa had higher abundances in only one or two timepoints. Broadly, ASVs classified as

Gammaproteobacteria *(Thalassotalea, Algicola*, *Alteromonas*) and Alphaproteobacteria *(Thalassobius, Shimia, Cognatishima*) typically have aerobic metabolisms and were more abundant during the timepoints T2 and T3. During timepoints T4 and T5, the community shifted to include strict anaerobes such as *Fusibacter* (class Clostridia) and *Halarcobacter* (class Campylobacteria) and facultative anaerobes like *Vibrio* (Figure 20).

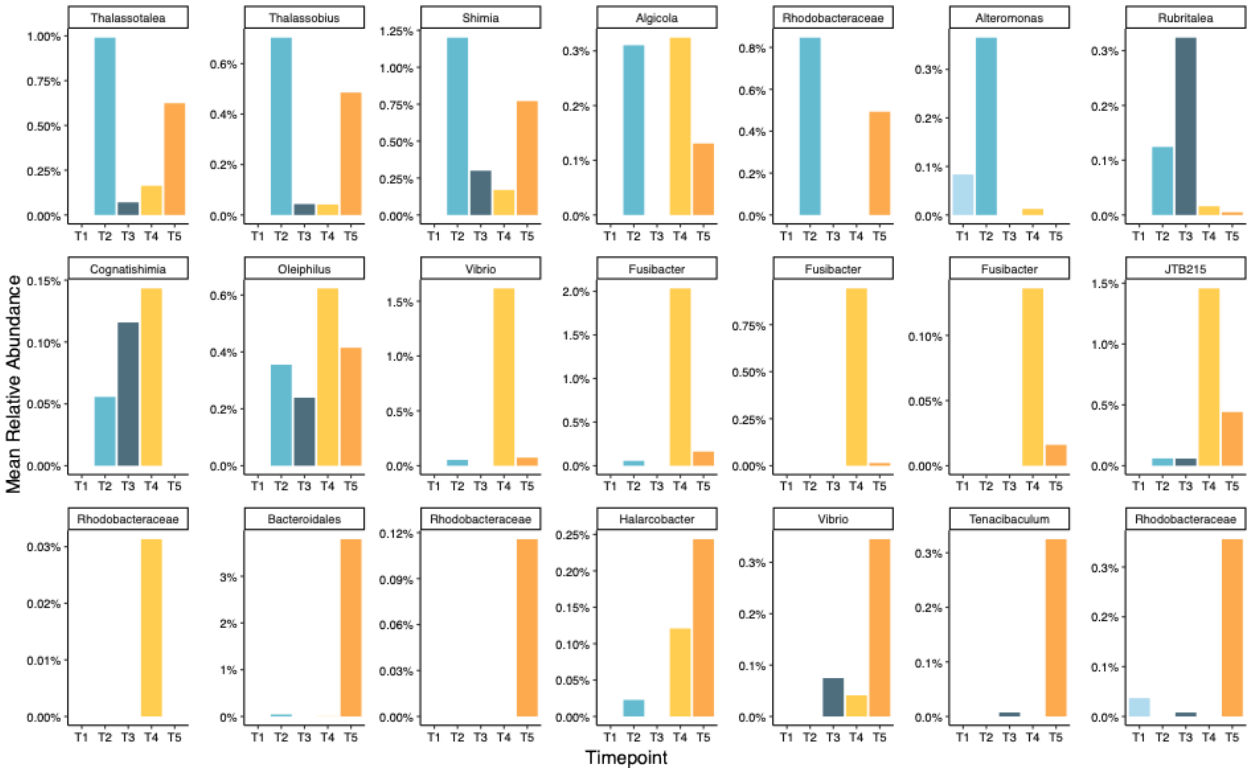

Figure 20. The relative abundances of 21 ASVs that were enriched in disease-exposed corals and have been previously associated with stony coral tissue loss disease. Bars are colored by timepoint during the experimental transmission study.

Quantification of the coral pathogen *Vibrio coralliilyticus* using digital PCR

Lastly, we successfully quantified the abundance of the coral pathogen *Vibrio coralliilyticus* using droplet digital PCR (ddPCR) using our previously designed assay (Ushijima et al., 2020). Previous aquaria-based trials demonstrated that the presence of this coral pathogen can exacerbate SCTLD infections (Ushijima et al., 2020). In the current experimental transmission study, most samples had a few copies of the *vcpA* gene per ng DNA, but one sample had 43 copies per ng DNA (Figure 21). No statistical differences in *vcpA* gene copy numbers were detected among health states (one-way ANOVA, $p > 0.05$).

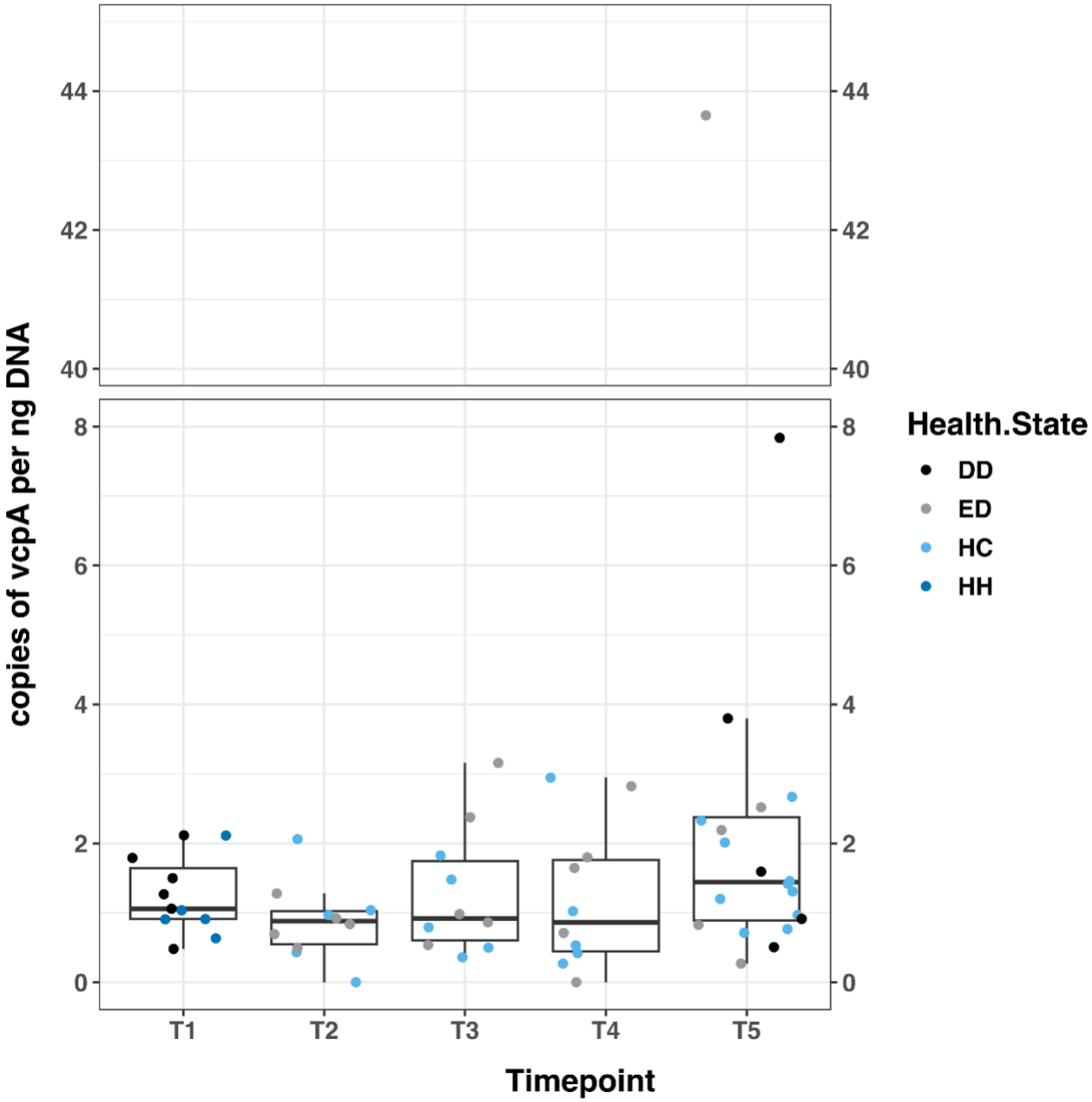

Figure 21. Copies of the *Vibrio coralliilyticus* vibriolysin-like *vcpA* gene per nanogram of DNA across timepoints in the experimental transmission of stony coral tissue loss disease. Points are colored by the health state of the coral where DD represents disease donor corals used to transmit disease, ED represents experimental corals exposed to disease, HC represents experimental corals exposed to healthy corals, and HH represents healthy naive corals before experimental exposures.

4.7. Task 7 – Image 10 corals from DRTO and begin analyzing the imaged corals (UNCW).

Samples were collected from the Dry Tortugas to track the fate of corals during the outbreak of SCTLD. Samples were collected before the disease was seen, denoted as the healthy health state (H), and then the same corals were sampled once SCTLD was present on the reefs. Two sample types were taken from these corals at timepoint 2 and 3 which included samples with the disease lesion (D) and samples on the same coral from the apparently healthy tissue (AH). In total, ten more samples were imaged for this 24-25 report, totaling 20 corals samples. Ten coral samples were analyzed utilizing ImageJ, focusing on the symbionts.

Some of the symbionts that were scored were removed from the analyses as the total set of paired samples have not been completed. In total, 100 endosymbionts, belonging to the three health states, were scored for the ten coral samples. The disease corals that had an active SCTLD diseased lesion had 75 symbionts scored (46 and T2 and 29 and T3), apparently healthy coral tissue on a disease colony (AH) totaled 12 (7 at T2 and 5 at T3), and healthy (H) totaled 13 (at T1). Overall, AH coral contained substantially less symbionts in these analyses from T2 and T3 when compared to D corals sample at those times, though these sample size differences are accounted for throughout statistical analyses.

The number of lipids within each symbiont was a significant factor in the dataset ($p = 0.00692l$; Fig 22). At T3, symbionts in D corals contained significantly more lipids than those in the AH corals ($p = 0.0014$). Furthermore, symbionts from D corals at T2 and T3 contained more lipids than those from H corals from T1 ($p = 0.0382$ (T2); $p = 0.0078$ (T3)). Regarding lipid size, AH at T3 contained smaller droplets than the D corals at T3 ($p = 0.0001$), and symbionts from D corals at T3 contained significantly larger lipids than at T2 ($p = 0.0002$; Fig 23). The symbionts from disease lesions tended to have more lipid droplets than the symbionts from the healthy corals or from the apparently healthy samples. The symbionts from diseased corals also had larger lipid droplets at T3, indicating that, though there was no increase in the number of lipids from T2 and T3, the size of the droplets increased. This could indicate that the lipid reserves increase in response to the onset of SCTLD and that they become larger as disease progresses. Further, this could also indicate a disruption in cellular metabolism through either increased lipid production triggered by stress or damage to cellular activity responsible for lipid breakdown caused by disease exposure.

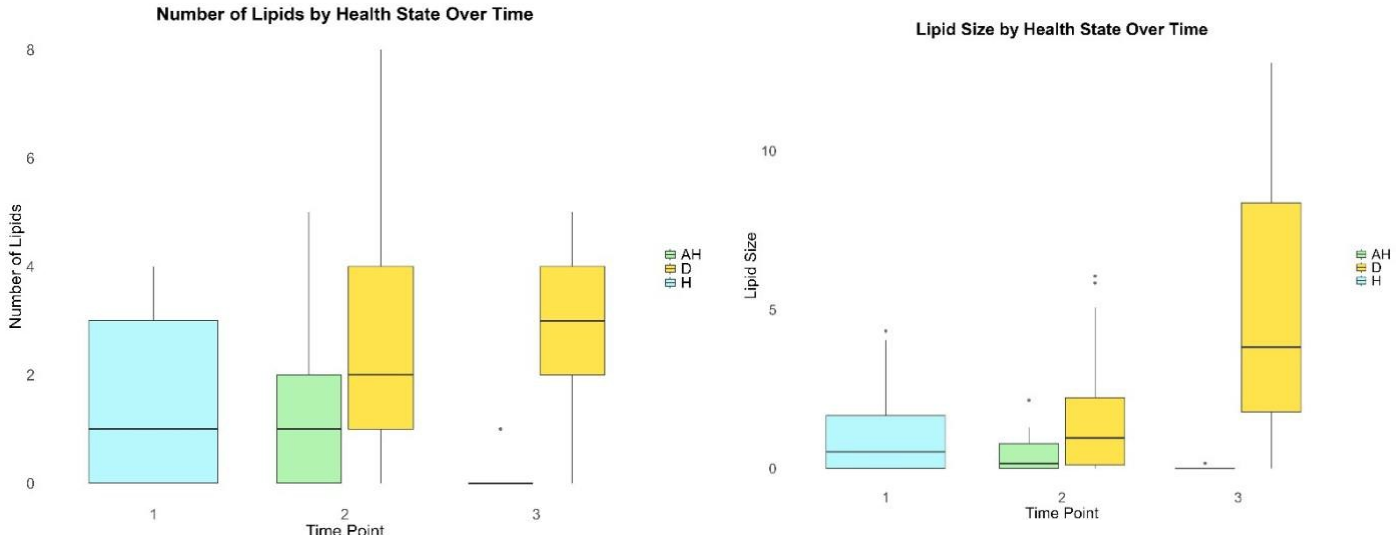

Figure 22. Boxplots of the number of lipids (left) and size of lipids (right) over time with the health state visualized by color.

Crystal presence (p = 0.00213) and size (p = 0.02) within the symbionts were both important parameters when analyzing coral health state and time point. The proportion of symbionts with crystals in D samples at T2 was lower than those at T3 (p = 0.0175) (Fig #). There was also a higher proportion of symbionts from D corals at T3 that contained crystals than H samples (p = 0.0083). Additionally, the D samples contained a larger crystal area (p = 0.0192) at T3 than T2, and D symbionts contained a larger crystal area than those in AH corals (p = 0.0304) at T2 and T3 (p = 0.0290) (Fig. #). Overall, an increase in crystals in the symbionts may be an ultrastructure indicator for SCTLD. In a well-functioning cell, metabolic waste products like uric acid should be excreted from the cell. However, as SCTLD progresses the symbionts may be accumulating these crystals due to cellular stress or symbiotic disruption. Understanding the rate at which crystal area increases could aid in further determining disease progression.

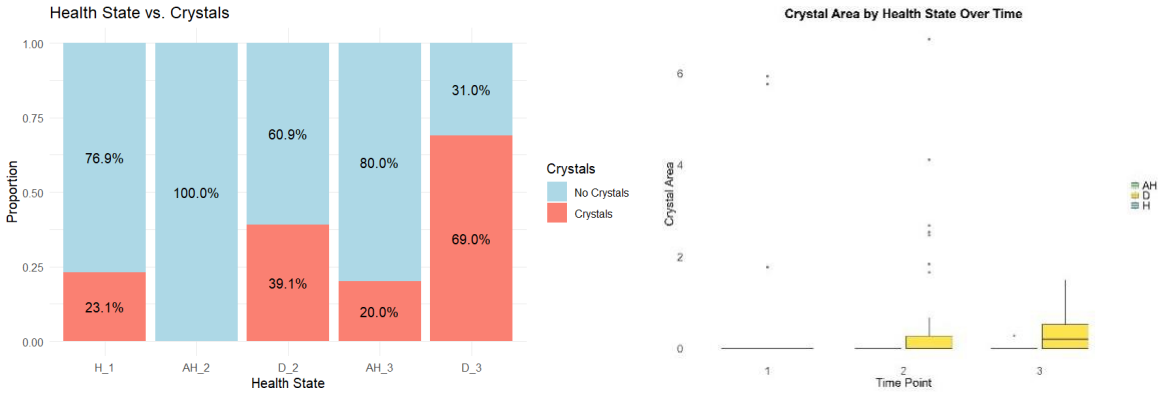

Figure 23: A proportion graph of the percent of symbionts that have crystals by health state and time (left). A boxplot of the total crystal area within the symbionts by time point with the health state visualized in different colors (right).

Though chloroplast breakdown was not statistically significant among the entire dataset (p = 0. 1233), symbionts from diseased samples reveal statistically higher proportions of cells with chloroplast breakdown in T3 compared to T2 (p = 0.032). This could be an indication of symbiont breakdown as SCTLD progresses, but a larger sample sized and further time points later in the SCTLD progression could provide a better understanding of this process. The presence of a viroplasm inside of these endosymbionts was rare – only one cell from an AH coral revealed this ultrastructure. However, the presence of viral-like particles (VLPs) was more common among the dataset with 45% of the symbionts containing them. The symbionts in AH from T2 contained the highest proportion of VLPs at 57.1%. However, there was no significant difference between health states and time points for this parameter, indicating that VLPs may not be related to SCTLD progression. A large proportion of symbiont cells in this dataset were morphologically symmetrical. For example, 100% of AH cells at T2. Overall, endosymbiont symmetry was common regardless of coral health state and does not seem to be an important factor when assessing SCTLD progression over time. Every other categorical parameter (e.g., the presence of accumulation bodies, electron dense bodies, separation from the cell wall and symbiosome, etc.) was not statistically significant within the symbionts from different health state or time points.

A Spearman correlation using numerical parameters (i.e., symbiont size, lipid number and size, starch number and size, and crystal area) across the entire dataset revealed symbiont cell size is positively correlated with factors, especially starch number and lipids (Fig. 24), and is least correlated with crystal area. Though starch number and size were not significant factors among the dataset, they were positively correlated with lipids. These correlations between size and number of storage granules need to be investigated further as it is unclear if the granules themselves are expanding the cell size or if the cell is increasing in size to make space for these structures. Interestingly, crystal area was not correlated with storage granules.

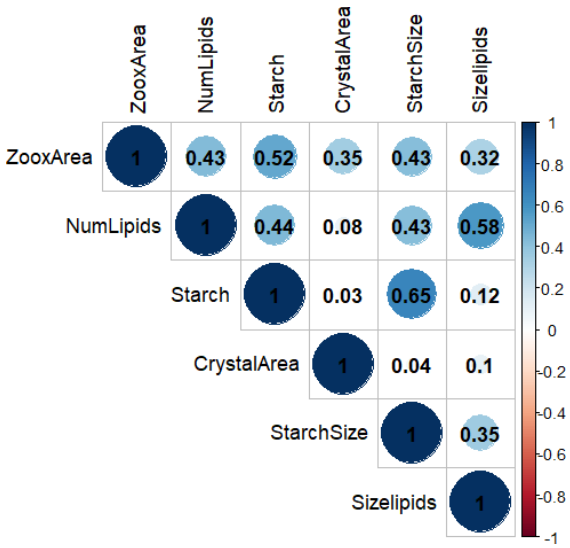

Figure 24. A Spearman correlation matrix for the entire dataset with just the numerical parameters. Blue indicates a positive correlation while red indicates a negative correlation with the numbers showing how closely correlated the parameters are.

Lastly, a Non-metric Multidimensional Scaling (NMDS) plot was constructed to visualize the degree of similarity between the symbionts scored in this dataset. Only

statistically significant numerical parameters were used to calculate the Bray-Curtis distance matrix. While symbionts from H and AH corals are more variable from one another, those from D corals tend to cluster at T2 and T3 (Fig. 25).

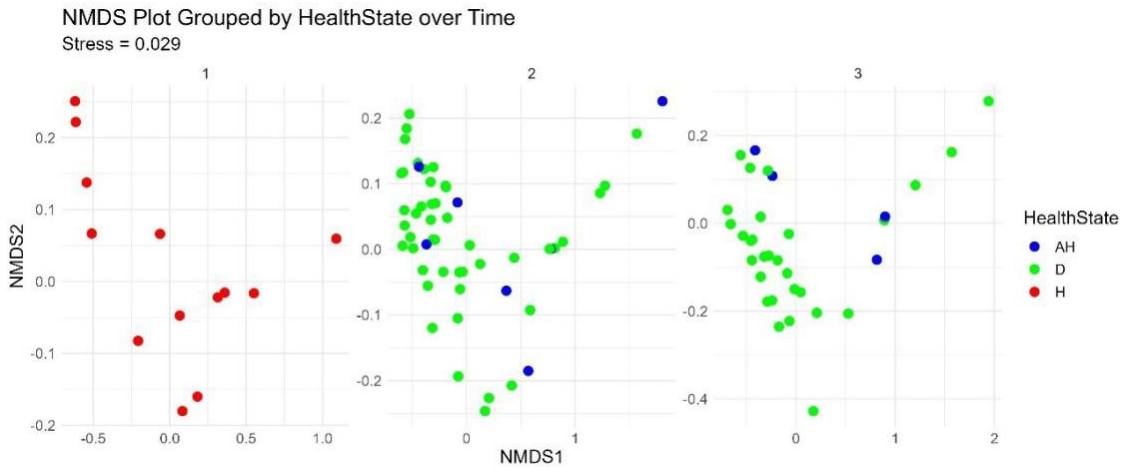

Figure 25. A Non-metric Multidimensional Scaling plot for each timepoint showing the health states by color.

4.8. Task 8 - Image 5 diseased *O. faveolata* samples with a potentially new coral disease observed in the Florida Keys (UNCW).

A total of 2 healthy samples, 4 disease unaffected samples, and 6 disease affected samples from 4 colonies, were imaged utilizing TEM, totaling 6 colonies between the three health states. Samples were taken from various locations, but only two locations have been images so far for this dataset. Additionally, disease affected samples were taken in replicate from the same lesion while only one sample for the disease unaffected tissue and the healthy coral were taken for this experimental design. In total, 209 zooxanthellae were scored, belonging to three health states – 22 symbionts were scored for healthy corals (H), 88 from disease unaffected corals (DU), and 99 from diseased (D) coral.

The number of starches within the symbionts was significant among the entire dataset (p = 3.394e-6). Symbionts from H corals had significantly fewer than D (p = 2.60e-7) and DU corals (p = 2.21e-5), but there was no significant difference between D and DU in the number of starches. Starch size was also significant among the dataset (p = 1.086e-6), with symbionts from D corals had larger starch than those in H (p = 8.11e-8) and DU (p = 0.0451). DU also had larger starch than H corals (p = 1.75e-5). The starch reserves increase in diseased corals, and they tend to get larger between the lesion and the adjacent apparently healthy tissue. This may indicate that there is higher photosynthetic activity or overproduction of glucose stores that cannot be properly utilized by the symbionts in response to disease. Additionally, it is also possible that because of acute tissue loss, the symbionts are storing extra granules in preparation for being released into the water column. This is a different trend seen from SCTLD samples where the number of starches decrease in disease, potentially indicating different physiological or cellular stress between these two possible diseases.

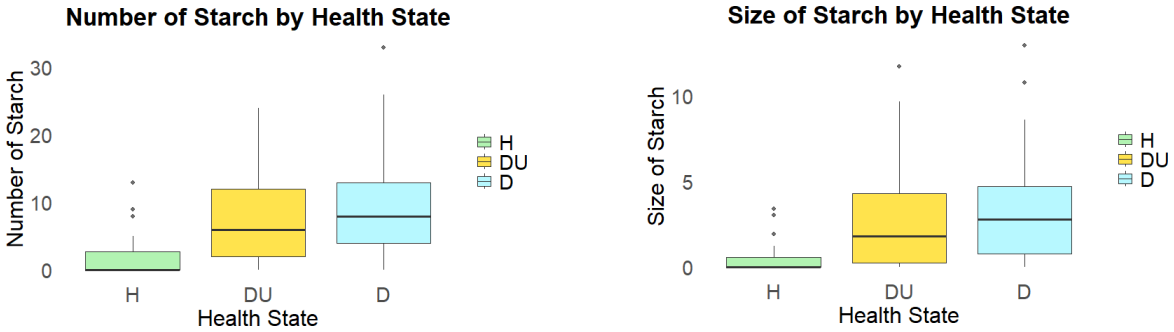

Figure 26. A boxplot of the number of starches by health state (left) and the size of the starches by health state (right). Color indicates the health state.

The number of lipids (p = 0.01) and size (p = 0.01) was a significant parameter across the dataset, with symbionts from D corals having greater (p = 0.0009) and larger lipids (p = 0.0022) than those from DU corals. The symbionts in diseased corals could potentially be storing lipids due to a utilization issue or to prepare for release, similar to starch findings. Symbionts from D corals also contained larger droplets (p = 0.0303) but interestingly not more than H corals. This could be due to H corals having a smaller sample size, so this relationship between health state and lipids may be further elucidated with further imaging.

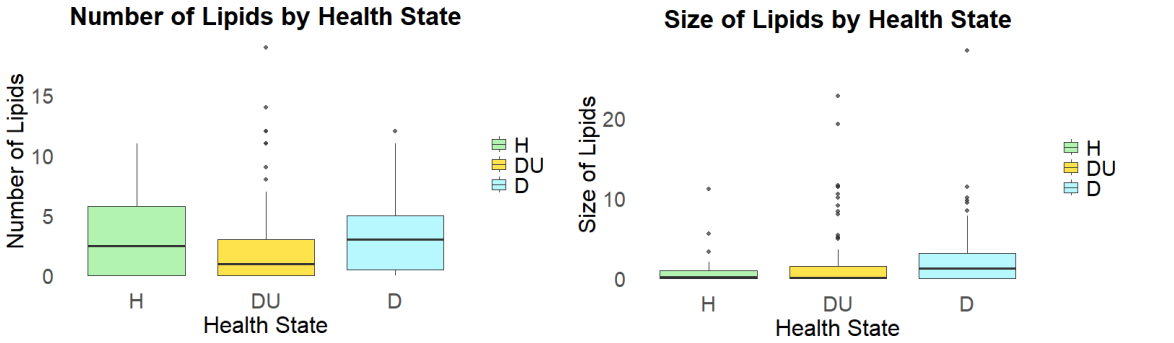

Figure 27: Boxplots of the number of lipids (left) and size of lipids (right) by health state.

Crystal presence (p = 0.0305) and crystal area (p = 0.03) were statistically significant across the dataset, with symbionts from DU corals having the lowest proportion and smallest size of crystals when compared to D (p = 0.0374; p = 0.0227) and H corals (p = 0.0247; p = 0.0117). The D corals did not have a significant difference in the presence or size between the healthy, which is a contrasting result seen for SCTLD samples.

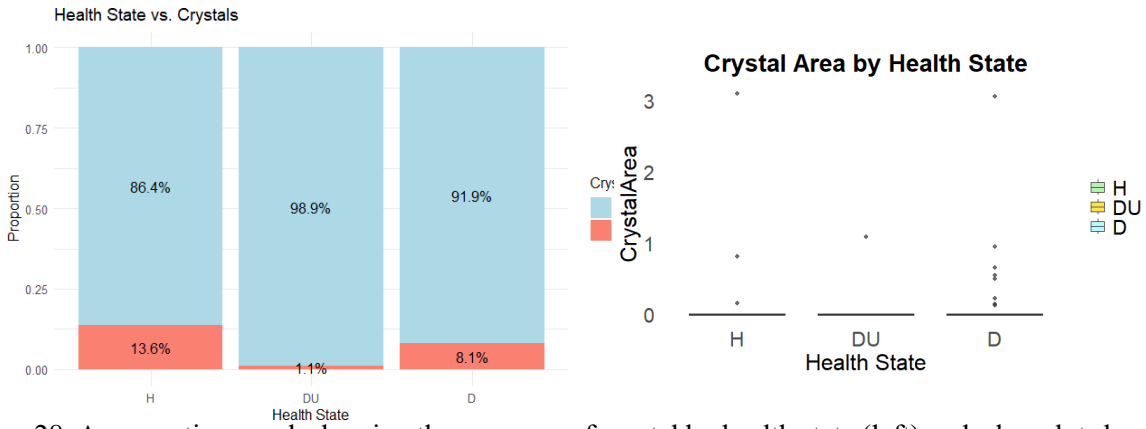

Figure 28. A proportion graph showing the presence of crystal by health state (left) and a boxplot showing the total area of the crystals by health state (right).

The symbiont cell size was another statistically significant parameter for health state (p = 0.02) with those from D corals being significantly larger than H (p = 0.0261) and DU corals (p = 0.0055). The cell size could be increasing due to stress from disease, or it could be accommodating the larger storage granules. Symbiont cell symmetry was a statistically significant parameter with regards to coral health state (p = 0.03462), with DU corals containing a lower proportion of symmetrical symbionts than D coral (p = 0.02345); however, is it not significant from H which may be due to the lower sample size. Understanding the cell symmetry needs to be investigated further to understand these trends regarding disease.

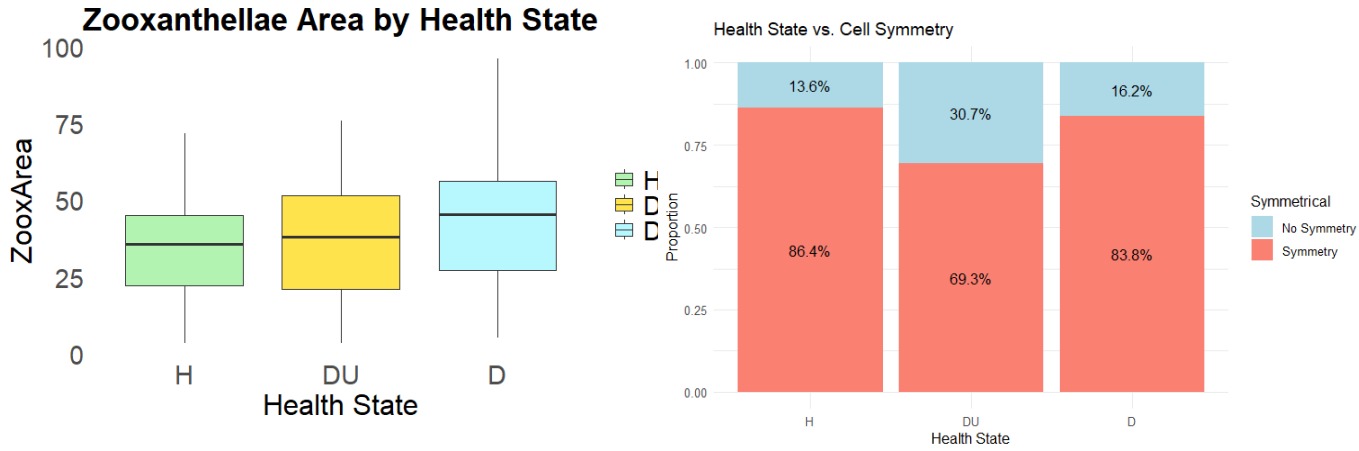

Figure 29. A boxplot a of the symbiont area by health state (left) and a proportion graph of the cell symmetry by health state (right).

Though the presence of accumulation bodies alone was not statistically significant among the dataset, accumulation body size was statistically significant between health states, with symbionts from the D health state contain smaller accumulation bodies than those from the H corals ($p = 0.0297$); the same trend is shown with the disease unaffected ($p = 0.0039$). This may be due to the sample size of the healthy corals, so continued analyses will aid in determining whether the presence of accumulation bodies is correlated to disease.

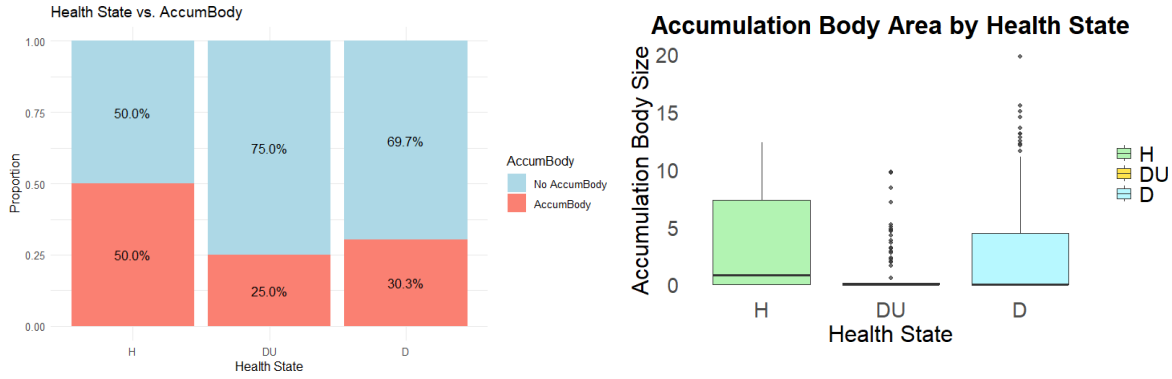

Figure 30. A proportion graph showing the presence of accumulation bodies by health state (left) and a boxplot showing the size of the accumulation bodies by health state (right).

The presence of electron dense bodies was also statistically significant across health states ($p = 6.512e\text{-}5$), with healthy corals containing a higher proportion of symbionts with these structures than disease unaffected corals ($p = 0.000212$) and those within diseased corals ($p = 0.0135$). The presence of VLPs within the endosymbionts was not statistically significant among coral health states. Additionally, other categorical parameters, including chloroplast breakdown, cell breakdown, pyrenoid, starch around

pyrenoid, thylakoid breakdown, separation from cell wall, separation from symbiosome, and cavity presence were not significant determinants of coral health state.

A Spearman correlation matrix reveals that starch and lipids are positively correlated to one another, as well as to the symbiont size. The number and size of starches are much more correlated to the size of the symbiont than the lipids, which could indicate that they are more tightly linked in physiology for this potential new disease. Crystals did not correlate to any numerical parameter in this study.

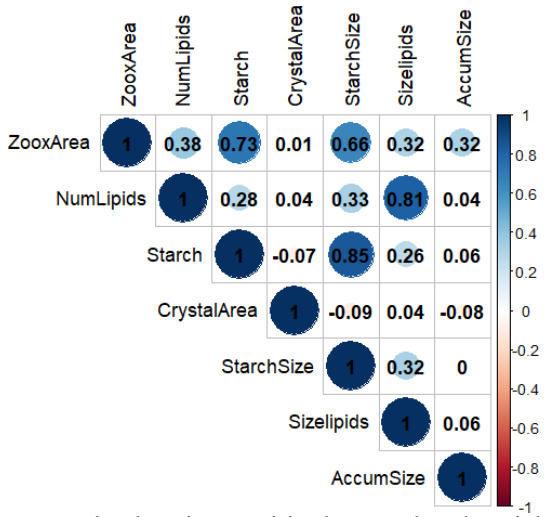

Figure 31. A Spearman correlation matrix showing positively correlated variables in blue and negatively correlated variables in red.

4.9. Host Immunity

This section is from Dr. Lauren Fuess, but was not directly funded by the grant this final report is for. This overview of what was done is only included for additional completeness.

Protein extraction: tissue is removed from coral frags using a painter's airbrush and a Tris buffer, then homogenized. These protein slurries are then used for the following assays.

Parameters measured:

- Melanin concentration
- Total phenoloxidase activity
- Phenoloxidase activity
- Catalase activity
- Peroxidase activity
- Antibacterial activity

Details:
Standardization of assays: Protein concentration is first measured from the protein slurries using a Red660 assay. This concentration is then used to standardize catalase, peroxidase, phenoloxidase, and total phenoloxidase activity assays. The melanin assay is run using a separate aliquot of the slurry that is dried and weighed and melanin concentration is standardized to tissue weight. Finally, for the antibacterial assay, the protein samples are all diluted to the lowest concentration sample and those diluted protein samples are used.
Melanin & melanin precursors: melanin concentrations are measured in each sample, and activity of total phenoloxidase & phenoloxidase, two precursor molecules in the melanin synthesis cascade, are measured as well to further characterize melanin production.
Melanin is an important innate immune molecule, particularly in invertebrates, as it acts in encapsulating pathogens and possibly wound healing.
Antibacterial assays: a live culture of *Vibrio coralliilyticus* strain Oft6-21 with pBU164, which is a plasmid transformed strain that expresses YFP, is added to the diluted protein homogenate from each sample, and bacterial growth is measured by the fluorescence emitted over several hours alongside a bacteria culture with no coral tissue to determine how much the coral protein is able to inhibit the growth of the bacteria (aka antibacterial activity). We calculate and report activity from this assay as both percent inhibition (% growth of culture in sample compared to no coral tissue control) as well as bacterial doubling time, for each sample.
Antioxidant assays: catalase and peroxidase activity are measured in each sample. Pathogen invasion, stress, and several immune pathways (i.e. melanin synthesis) result in the production of reactive oxygen species (ROS) which are harmful to coral tissue if left unchecked. So, antioxidants are often produced by the coral during times of stress or infection to remove these ROSs.

More detailed methods for these assays can also be found in Pinzon et al. 2014, "Relationship between phylogeny and immunity suggests older Caribbean coral lineages are more resistant to disease"

5. DISCUSSION AND MANAGEMENT RECOMMENDATIONS

5.1. Discussion

5.1.1. Transcriptomics and Proteomics

For viral identification, the immediate next steps are to compare geNomad and RdRP-Search according to the plans mentioned above and possibly assess the performance of additional tools currently being released in real-time. Once we have a confident set of true RNA viruses, we plan on employing a taxonomic and functional gene annotation workflow, as well as a host-prediction workflow originally conducted in Zayed et al. 2022. The overarching plan is to assess what the taxonomic identities of viral populations are associated with diseased vs. non-diseased conditions, what they may be doing functionally, and if these viruses are predicted to have a coral or endosymbiont host.

In order to explore the potential viral contributors to SCTLD disease susceptibility, transmission, and disease development, we compared the predicted viral communities present in three datasets, CNAT_1, OFAV1, OFAV2. The high confidence viral protein hits were extracted from BLASTP results and summarized across samples. A subset of viral families was extracted that identified several viral hits present in both CNAT1 and OFAV2 but absent from OFAV1. These viral family hits had relatively low abundance, but may suggest variation in disease progress, environmental exposure, and susceptibility. However, given the relatively limited number of viral families identified, and the large taxonomic diversity, further investigation is needed to determine if these differences are a) consistent across different experimental tanks (1E, 2E, 3E, ect), b) differ in the control tanks, c) and how the virome changes across other timepoint i.e Timepoint 3, Timepoint 4, Timepoint 5. The proteome data will serve to verify potential viruses found in the transcriptome dataset, and in the DNA datasets. We aim to uncover additional factors contributing to disease including pathogenic bacterial co-infections, environmental stressors, tank-specific stressors, all which may contribute to the complex disease dynamics of SCTLD. Overall, there are no viral signatures that immediately stand out as potential agents, but continued integration with the other datasets is necessary to make any conclusive statements.

5.1.2. Metabolomics

To investigate how corals respond metabolically to SCTLD, the chemical profiles (metabolomes) of several coral species was investigated. Due to strong species-specific differences, the analysis focused on *Montastraea cavernosa* to reduce variability. Analysis showed that metabolite alpha diversity in SCTLD-exposed fragments dropped significantly at 48 hours post-exposure (SP2) and gradually increased over time, a trend not observed in healthy controls. The most distinct separation between healthy and diseased samples occurred at SP2—before visible signs appeared—suggesting a rapid early metabolic response to SCTLD.

Further statistical analysis confirmed significant differences between healthy and diseased samples only at SP2. A total of 222 metabolite features contributed to differences across all time points, with SP2 and the final sampling period (SP5) showing the highest number of unique features. This indicates that different metabolic processes are active during early and late stages of disease progression.

Key metabolites identified included lyso-platelet-activating factors (lyso-PAF), acylcarnitines (CAR), and diacylglyceryl-carboxyhydroxymethylcholine (DGCC). Lyso-PAF, a lipid involved in inflammation, was consistently elevated in diseased samples and may play a role in the coral's immune response. CARs, which are involved in fatty acid metabolism and mitochondrial function, were also more abundant in SCTLD-exposed corals, suggesting metabolic stress or dysfunction. DGCC lipids, derived from the coral's algal symbionts, showed altered abundance, possibly reflecting membrane stress or damage in the symbionts.

Additional algal-derived lipids, such as MGDG and DGDG— potentially key components of the photosynthetic machinery—were also differentially abundant, indicating potential impairment of photosynthesis during infection. These findings suggest that both the coral host and its symbiotic algae undergo significant metabolic changes in response to SCTLD, with distinct compounds involved at different stages of disease. The early detection of unique

metabolites before visible signs highlight the potential for identifying biomarkers for early diagnosis and monitoring of coral health.

5.1.3. Histology

Apparent SCTLD was histologically confirmed in all DD samples (CNAT, OFAV and MCAV). Fragments exposed to these colonies in genotype-specific separate aquaria developed SCTLD lesions or were diagnosed with suspect SCTLD in the naïve OFAV and MCAV that were exposed to the disease donor colonies. The current case definition of SCTLD was applied, based on histopathological changes, including the presence of lytic necrosis in gastrodermis associated with necrosis and degenerative changes in endosymbionts [38].

Not all fragments responded the same during the experiment, although they were cut from the same genotype colony and in the same tank. This has been noted in other coral experiments. Field observations on bleaching corals have reported variations in paling to completely bleached patches of tissues within a colony, suggesting that the particular polyps' gastrodermal cells may have been infected with different clades (now species) of the endosymbionts. The differential susceptibility of the zooxanthellae to whatever was causing the bleaching (e.g., elevated seawater temperature) resulted in different responses within the host cells, which could lead to variations in the production of photosynthetic products, functioning of the symbiosis, and pathological changes. Once a colony is fragmented, the individual fragments can respond differently. Perhaps the data from the other analyses performed on these fragments will enlighten our understanding of this histological observation.

The emergence of globules among degraded granular amoebocytes in the mesenteries attached to the filaments was notable in the disease-exposed MCAV, as well as in the donor specimens (CNAT, OFAV, and OFRA); these globules were not reported in Landsberg et al. (2020). These species differ in the distribution, morphology, and probably the composition of the proteins filling the vesicles in granular amoebocytes (suspected to be enzymes for defending the host coral from microbes), although more study is required. Although globules were not observed in disease-exposed OFAV specimens, the response found in disease-exposed MCAV and in diseased donor DD species is presumably attributable to SCTLD as the process of cellular necrosis proceeds. These globules are presumably residual bodies resulting from lysosomal self-autolysis activity, potentially leading to rapid tissue necrosis. Similar pathological changes were recently observed in an OFAV disease study (*Orbicella* acute tissue loss disease, OATLD; note that TEM results of this study are presented in Task 8 of this report).

A main concern from the histology results of this study is that naïve HH and HC MCAV and OFAV specimens exhibited some pathological changes in their tissues, including epithelial atrophy and cell loss, endosymbiont necrosis and loss, lysing mucocytes, fragmentation of the polyps' basal body walls, and separation of the gastrodermis from the mesoglea along the surface body walls. Specimens from which the fragments were taken had been maintained in the Smithsonian Marine Station's aquarium for several years following their collection from Florida reefs. During this time, they were fed 2 times per week. After fragmentation, the pieces were returned to the aquaria they had been in to recover for 12 days, during which they were fed at the same

frequency with *Dr. G's* product line and supplemented with *Three Little Fishes* (enriched food that included zooplankton) and extended their polyps during feeding (normal behavior). When the experiment started, feeding of the fragments in all the aquaria stopped because of concern that food remnants would have fouled the water. In addition, the seawater was filtered and exposed to UV-light to reduce viral and bacterial loads. These conditions continued throughout the 41-day study period during which all samples were collected.

It is likely that starvation or malnourishment contributed to tissue degradation across the HC and ED tanks, potentially affecting endosymbiont condition (note also that changes in PAS reactions over the course of study support Task 5, TEM analysis in this report), as well as the host's development, necrosis, and lysing of mucocytes and other cells and appearance of the SCTLD lesions. Multiple studies have confirmed that all scleractinian corals require feeding with sources of nitrogen- and phosphorus-containing protein, especially the larger-polyped species such as CNAT, MCAV, and OFAV (Goldberg, 2018). The ideal feeding regime has been noted to be 3 times per week, as reported by Szmant-Froelich and Pilson (1980) to maintain coral tissue composition close to what was found in the field, even for small-polyped corals (Ferrier-Pages et al., 2003). Elevated temperature and toxicity tests of corals have recommended feeding during testing for periods greater than 4 to 7 days (acute and short-duration studies). Grottoli et al. (2021) noted that "supplemental feeding at least once a week to satiation provides corals with some of that essential nutrition (though coral have access to zooplankton nightly on the reef, so up to three times a week is more realistic; Tables 1; Appendix S1: Section S1.5)" for heat-stress experiments longer than 8 days. Barker et al. (2025, preprint) reported for sunscreen toxicity testing protocols that feeding should be performed 3 times per week (in their Table 2). During the test, uneaten food particles would be removed by vacuuming and the tanks topped off with clean seawater after feeding, for a 10-15% water replacement. This protocol should have mitigated any concerns about water fouling during this study.

When corals are not fed proteins and are expected to survive with only exposure to light for the endosymbionts, they are not able to synthesize all of the necessary compounds in their cells [39]. This was increasingly evident during the time series sampling in the decrease in cytoplasmic staining intensity with eosin, which binds to proteins, in the tissue sections of this study (in both coral samples and endosymbionts). This was further supported in the degradation of contractile myoneme extensions of the epitheliomuscular cells, mesoglea, and granular amoebocytes, with loss of nematocysts, granular digestive gland cells in the cnidoglandular bands, and other adverse changes that would reduce coral survival whether exposed to DD fragments or not. Overall, this experiment has provided insights into the development of SCTLD and post-mortem changes in corals. Investigations of the food quality, feeding regimes, and ability of sick corals to feed on reef areas affected by SCTLD outbreaks may help determine whether these aspects of heterotrophy also have a role in the development of this disease in affected species, and potentially inform on patterns of susceptibility among coral species.

5.1.4. TEM

5.1.4.1. Holistic Time Series

A total of 122 symbionts were analyzed across three coral health states—naïve (HH), exposed to disease (ED), and healthy controls (HC)—and five time points to assess cellular and subcellular changes in response to SCTLD. Symbiont cell size varied significantly among groups, with larger cells observed in ED and HC samples at time point 2 (T2) compared to later stages, though small sample sizes at T2 may have influenced these results.

Starch content showed significant differences. ED samples at T2 had more and larger starch granules than at later time points, suggesting an early accumulation of energy reserves. However, starch content declined over time in ED samples, a trend also observed in field samples. Comparatively, HC and HH samples maintained higher starch levels and larger granules than ED samples at T3–T5, indicating a potential metabolic disruption in diseased corals.

Lipid content also differed significantly. ED samples at T2 had more and larger lipid bodies than at T4 and T5, while HC samples had more lipids than ED at T5. Naïve corals consistently had more and larger lipids than ED samples at several time points, suggesting that lipid reserves diminish more rapidly in diseased corals. These trends point to a depletion of energy stores (i.e., lipids) as SCTLD progresses.

Crystalline structures were only observed in ED samples at T4 and T5, with significant differences in both presence and area. Their predominant appearance in diseased samples suggests a potential link to SCTLD pathology.

VLPs were significantly more common in ED samples at T2, T4, and T5 compared to HH at T1, though no significant differences were found between HC and ED samples. This suggests VLP presence may be influenced by environmental or experimental conditions rather than disease alone.

Algal symbiont traits became more distinct and tightly clustered by health state over time. While electron-dense bodies were statistically significant overall, no pairwise differences were found. Other ultrastructural features, like thylakoid and chloroplast breakdown, were not significantly different across groups.

5.1.4.2. DRTO Time Series

Samples were collected from the Dry Tortugas before and after disease onset. Corals were sampled at three health states: healthy (H), diseased lesion tissue (D), and apparently healthy tissue on diseased colonies (AH), across two time points (T2 and T3). Ten additional coral samples were analyzed for this report, totaling 20 samples, with 100 symbionts scored.

Significant differences were observed in lipid content. Symbionts from D samples had more lipids than those from AH samples at T3 ($p = 0.0014$) and more than H samples at both T2 and T3. Lipid droplet size was also larger in D samples at T3 compared to both AH and earlier D samples, suggesting lipid accumulation as disease progresses. This may reflect a stress response or impaired lipid metabolism due to SCTLD.

Crystal presence and size were also significant. D samples at T3 had more symbionts with crystals and larger crystal areas than at T2 and compared to AH and H

samples. These crystals may represent waste accumulation due to disrupted cellular function, potentially serving as an ultrastructural marker of disease progression.

Chloroplast breakdown was not significant overall but increased in D samples from T2 to T3 ($p = 0.032$), indicating possible symbiont degradation as SCTLD advances. Viral-like particles (VLPs) were present in 45% of algal symbionts, with the highest proportion in AH corals at T2, though no significant differences were found between health states or time points. This suggests VLP presence may not be directly linked to SCTLD.

Other ultrastructural features (e.g., electron-dense bodies, separation from cell wall, chloroplast breakdown) were not significantly different across groups. Symbiont size was positively associated with lipid and starch content, though crystal area was not correlated with storage granules.

Symbionts from D samples clustered more tightly over time, while those from H and AH samples remained more variable. These findings suggest that SCTLD induces measurable changes in symbiont ultrastructure, particularly in lipid and crystal dynamics, which may serve as indicators of disease progression.

5.1.4.3. *Orbicella* Acute Tissue Loss Disease

Transmission electron microscopy (TEM) was used to examine 209 algal symbionts from six coral colonies across three health states: healthy (H), disease unaffected (DU), and disease affected (D). Samples were collected from two reef locations, with D samples taken in replicate from lesions, while H and DU samples were single replicates. Symbionts analyzed included 22 from H, 88 from DU, and 99 from D corals.

Starch content was significantly different across health states. Symbionts from H samples had fewer and smaller starch granules than those from D and DU samples. D samples had the largest starch granules, suggesting increased photosynthetic activity or impaired glucose utilization. This trend contrasts with SCTLD, where starch typically decreases, indicating potentially different disease mechanisms.

Lipid number and size were also significantly higher in D samples compared to DU, with larger droplets observed in D than H samples. This may reflect lipid accumulation due to metabolic stress or preparation for symbiont expulsion. However, the lack of difference in lipid number between D and H may be influenced by the smaller H sample size.

Crystal presence and area were significantly greater in D and H samples compared to DU. This suggests that crystal accumulation may be linked to stress or waste retention, though the pattern differs from SCTLD, where diseased samples typically show more crystals than healthy ones.

Symbiont cell size was significantly larger in D samples, potentially due to storage granule accumulation or disease-related stress. Accumulation body size was smaller in D samples compared to H and DU, while electron-dense bodies were more common in H samples than in DU and D, suggesting a decline in cellular integrity with disease.

VLPs were observed in some algal symbionts but were not significantly different across health states. Other ultrastructural features, including chloroplast breakdown and thylakoid separation, were not significant.

There were strong positive relationships between symbiont size, starch, and lipid content, suggesting coordinated changes in energy storage. Crystal area, however, was not correlated with other parameters. These findings highlight distinct ultrastructural changes in symbionts associated with disease and suggest a different physiological response than that observed in SCTLD.

5.1.5. Microbiome

Host-associated microbiomes have the capacity to change rapidly, especially in response to disturbances like disease. The most important feature of the current study is the repeated sampling of coral microbiomes over the course of disease transmission, in comparison to control corals exposed to healthy corals in an aquarium setting. Here, as anticipated, we detected changes in the coral microbiome over time. For the first time, we were also able to demonstrate changes in the relative abundances of taxa previously associated with SCTLD over time after exposure to disease. As disease progressed, SCTLD-associated bacteria with anaerobic metabolisms were enriched, suggesting their role as opportunistic or secondary pathogens that are favored in decaying tissue. *Vibrio coralliilyticus* was at low abundance throughout the study and is thus not playing a role in disease progression in this experimental transmission. Our next steps include integration and interpretation of these data with other datasets generated by collaborators.

5.1.6. Next Steps

Multiple research groups have collaborated to generate extensive datasets derived from a standardized collection of samples, utilizing laboratory-infected naïve corals across multiple timepoints. This represents a significant and unprecedented undertaking in the field. While the project has successfully produced a substantial volume of data, the next critical step involves the integration and synthesis of these diverse datasets into a cohesive whole. Additionally, certain analyses—such as transmission electron microscopy (TEM)—remain incomplete due to their time-intensive nature. Over the coming year, the primary objective will be to conduct comparative analyses across datasets to derive meaningful conclusions.

5.2. Management Recommendations

1) This project generated a comprehensive baseline dataset of naïve, healthy corals, which serves as an important reference for assessing the impacts of future disturbances. Due to the project's holistic methodology, the dataset holds value not only for studying disease-related events but also for understanding a broad range of environmental stressors.

2) Several of the datasets suggest that significant changes to the host metabolome, microbiome, and cellular structures change before any gross signs of disease are visible. This can be further investigated as potential diagnostic tools to detect SCTLD in corals that might not present any gross disease signs.

3) We have not identified any overwhelming evidence for a specific viral pathogen associated with SCTLD. VLP abundance observed in disease versus healthy samples was not significantly different nor where any viral sequences have been

indicated in our data. While this does not conclusively demonstrate viruses are not involved, there still requires more integration with the other data sets to make can conclusive statements.

4) Preliminary transmission electron microscopy (TEM) data from *Orbicella faveolata* samples (Task 8) suggest that the observed cellular pathologies may represent a distinct condition rather than a variant of SCTLD. This emerging condition, currently termed *Orbicella* acute tissue loss disease (OATLD), could pose an additional and significant threat to Florida's coral reef ecosystems. Given the rapid progression of tissue loss and the current lack of understanding regarding its etiology, we strongly recommend continued and focused investigations into OATLD.

6. REFERENCES CITED

1. Aeby GS, Ushijima B, Campbell JE, Jones S, Williams GJ, Meyer JL, Häse C, Paul VJ (2019) Pathogenesis of a Tissue Loss Disease Affecting Multiple Species of Corals Along the Florida Reef Tract. *Frontiers in Marine Science*, 6(678)https://doi.org/10.3389/fmars.2019.00678

2. Muller EM, Sartor C, Alcaraz NI, Woesik R van (2020) Spatial Epidemiology of the Stony-Coral-Tissue-Loss Disease in Florida. *Frontiers in Marine Science*, 7:163. https://doi.org/10.3389/fmars.2020.00163

3. Meiling SS, Muller EM, Lasseigne D, Rossin A, Veglia AJ, MacKnight N, Dimos B, Huntley N, Correa AMS, Smith TB, Holstein DM, Mydlarz LD, Apprill A, Brandt ME (2021) Variable Species Responses to Experimental Stony Coral Tissue Loss Disease (SCTLD) Exposure. *Frontiers in Marine Science*, 8:670829. https://doi.org/10.3389/fmars.2021.670829

4. Meyer JL, Castellanos-Gell J, Aeby GS, Häse C, Ushijima B, Paul VJ (2019) Microbial community shifts associated with the ongoing stony coral tissue loss disease outbreak on the Florida Reef Tract. *Frontiers in Microbiology*, 10(2244)https://doi.org/10.3389/fmicb.2019.02244

5. Rosales SM, Clark AS, Huebner LK, Ruzika RR, Muller EM (2020) Rhodobacterales and Rhizobiales Are Associated With Stony Coral Tissue Loss Disease and Its Suspected Sources of Transmission. *Frontiers in Microbiology*, 11:20. https://doi.org/10.3389/fmicb.2020.00681

6. Becker CC, Brandt M, Miller CA, Apprill A (2021) Microbial bioindicators of Stony Coral Tissue Loss Disease identified in corals and overlying waters using a rapid field-based sequencing approach. *Environmental Microbiology*, :1462-2920.15718. https://doi.org/10.1111/1462-2920.15718

7. Neely KL, Macaulay KA, Hower EK, Dobler MA (2020) Effectiveness of topical antibiotics in treating corals affected by Stony Coral Tissue Loss Disease. *PeerJ*, 8(e9289)https://doi.org/10.7717/peerj.9289

8. Shilling EN, Combs IR, Voss JD (2021) Assessing the effectiveness of two intervention methods for stony coral tissue loss disease on Montastraea cavernosa. *Scientific Reports*, 11(1):8566. https://doi.org/10.1038/s41598-021-86926-4

9. Walker BK, Turner NR, Noren HKG, Buckley SF, Pitts KA (2021) Optimizing Stony Coral Tissue Loss Disease (SCTLD) Intervention Treatments on Montastraea cavernosa in an Endemic Zone. *Frontiers in Marine Science*, 8:666224. https://doi.org/10.3389/fmars.2021.666224

10. Ushijima B, Meyer JL, Thompson S, Pitts K, Marusich MF, Tittl J, Weatherup E, Reu J, Wetzell R, Aeby GS, Häse CC, Paul VJ (2020) Disease Diagnostics and Potential Coinfections by Vibrio coralliilyticus During an Ongoing Coral Disease

Outbreak in Florida. *Frontiers in Microbiology*, 11:569354. https://doi.org/10.3389/fmicb.2020.569354

11. Work TM, Weatherby TM, Landsberg JH, Kiryu Y, Cook SM, Peters EC (2021) Viral-Like Particles Are Associated With Endosymbiont Pathology in Florida Corals Affected by Stony Coral Tissue Loss Disease. *Frontiers in Marine Science*, 8:750658. https://doi.org/10.3389/fmars.2021.750658

12. Wilson W, Francis I, Ryan K, Davy S (2001) Temperature induction of viruses in symbiotic dinoflagellates. *Aquatic Microbial Ecology*, 25:99–102. https://doi.org/10.3354/ame025099

13. Lohr J, Munn CB, Wilson WH (2007) Characterization of a Latent Virus-Like Infection of Symbiotic Zooxanthellae. *Applied and Environmental Microbiology*, 73(9):2976–2981. https://doi.org/10.1128/AEM.02449-06

14. Thurber RV, Willner-Hall D, Rodriguez-Mueller B, Desnues C, Edwards RA, Angly F, Dinsdale E, Kelly L, Rohwer F (2009) Metagenomic analysis of stressed coral holobionts. *Environmental Microbiology*, 11(8):2148–2163. https://doi.org/10.1111/j.1462-2920.2009.01935.x

15. Beurmann S, Ushijima B, Videau P, Svoboda CM, Smith AM, Rivers OS, Aeby GS, Callahan SM (2017) Pseudoalteromonas piratica strain OCN003 is a coral pathogen that causes a switch from chronic to acute Montipora white syndrome in Montipora capitata. *PLOS ONE*, 12(11):e0188319. https://doi.org/10.1371/journal.pone.0188319

16. Cooney RP, Pantos O, Tissier MDL, Barer MR, Bythell JC (2002) Characterization of the bacterial consortium associated with black band disease in coral using molecular microbiological techniques. *Environmental Microbiology*, 4(7):401–413.

17. Meyer JL, Gunasekera SP, Scott RM, Paul VJ, Teplitski M (2016) Microbiome shifts and the inhibition of quorum sensing by Black Band Disease cyanobacteria. *The ISME journal*, 10(5):1204–1216.

18. Charon J, Olendraite I, Forgia M, Chong LC, Hillary LS, Roux S, Kupczok A, Debat H, Sakaguchi S, Tahzima R, Nakagawa S, Babaian A, Abroi A, Bejerman N, Ben Mansour K, Brown K, Butkovic A, Cervera A, Charriat F, Chen G, Chiba Y, De Coninck L, Demina T, Dominguez-Huerta G, Dubrulle J, Gutierrez S, Harvey E, Jayaraj Mallika FR, Karapliafis D, Lim SJ, Kasibhatla SM, Mifsud JCO, Nishimura Y, Ortiz-Baez AS, Raco M, Rivero R, Sadiq S, Saghaei S, San JE, Shaikh HM, Sieradzki ET, Sullivan MB, Sun Y, Wille M, Wolf YI, Zrelovs N, Neri U (2024) Consensus statement from the first RdRp Summit: advancing RNA virus discovery at scale across communities. *Frontiers in Virology*, 4:1371958. https://doi.org/10.3389/fviro.2024.1371958

19. Wolf YI, Kazlauskas D, Iranzo J, Lucía-Sanz A, Kuhn JH, Krupovic M, Dolja VV, Koonin EV (2018) Origins and Evolution of the Global RNA Virome. *mBio*, 9(6):e02329-18. https://doi.org/10.1128/mBio.02329-18

20. Zayed AA, Wainaina JM, Dominguez-Huerta G, Pelletier E, Guo J, Mohssen M, Tian F, Pratama AA, Bolduc B, Zablocki O, Cronin D, Solden L, Delage E, Alberti A, Aury J-M, Carradec Q, Da Silva C, Labadie K, Poulain J, Ruscheweyh H-J, Salazar G, Shatoff E, Tara Oceans Coordinators‡, Bundschuh R, Fredrick K, Kubatko LS, Chaffron S, Culley AI, Sunagawa S, Kuhn JH, Wincker P, Sullivan MB, Acinas SG, Babin M, Bork P, Boss E, Bowler C, Cochrane G, De Vargas C, Gorsky G, Guidi L, Grimsley N, Hingamp P, Iudicone D, Jaillon O, Kandels S, Karp-Boss L, Karsenti E, Not F, Ogata H, Poulton N, Pesant S, Sardet C, Speich S, Stemmann L, Sullivan MB, Sungawa S, Wincker P (2022) Cryptic and abundant marine viruses at the evolutionary origins of Earth's RNA virome. *Science*, 376(6589):156–162. https://doi.org/10.1126/science.abm5847

21. Camargo AP, Roux S, Schulz F, Babinski M, Xu Y, Hu B, Chain PSG, Nayfach S, Kyrpides NC (2024) Identification of mobile genetic elements with geNomad. *Nature Biotechnology*, 42(8):1303–1312. https://doi.org/10.1038/s41587-023-01953-y

22. Keeling PJ, Burki F, Wilcox HM, Allam B, Allen EE, Amaral-Zettler LA, Armbrust EV, Archibald JM, Bharti AK, Bell CJ, Beszteri B, Bidle KD, Cameron CT, Campbell L, Caron DA, Cattolico RA, Collier JL, Coyne K, Davy SK, Deschamps P, Dyhrman ST, Edvardsen B, Gates RD, Gobler CJ, Greenwood SJ, Guida SM, Jacobi JL, Jakobsen KS, James ER, Jenkins B, John U, Johnson MD, Juhl AR, Kamp A, Katz LA, Kiene R, Kudryavtsev A, Leander BS, Lin S, Lovejoy C, Lynn D, Marchetti A, McManus G, Nedelcu AM, Menden-Deuer S, Miceli C, Mock T, Montresor M, Moran MA, Murray S, Nadathur G, Nagai S, Ngam PB, Palenik B, Pawlowski J, Petroni G, Piganeau G, Posewitz MC, Rengefors K, Romano G, Rumpho ME, Rynearson T, Schilling KB, Schroeder DC, Simpson AGB, Slamovits CH, Smith DR, Smith GJ, Smith SR, Sosik HM, Stief P, Theriot E, Twary SN, Umale PE, Vaulot D, Wawrik B, Wheeler GL, Wilson WH, Xu Y, Zingone A, Worden AZ (2014) The Marine Microbial Eukaryote Transcriptome Sequencing Project (MMETSP): Illuminating the Functional Diversity of Eukaryotic Life in the Oceans through Transcriptome Sequencing. *PLoS Biology*, 12(6):e1001889. https://doi.org/10.1371/journal.pbio.1001889

23. Li C-X, Shi M, Tian J-H, Lin X-D, Kang Y-J, Chen L-J, Qin X-C, Xu J, Holmes EC, Zhang Y-Z (2015) Unprecedented genomic diversity of RNA viruses in arthropods reveals the ancestry of negative-sense RNA viruses. *eLife*, 4:e05378. https://doi.org/10.7554/eLife.05378

24. Krishnamurthy SR, Janowski AB, Zhao G, Barouch D, Wang D (2016) Hyperexpansion of RNA Bacteriophage Diversity. *PLOS Biology*, 14(3):e1002409. https://doi.org/10.1371/journal.pbio.1002409

25. Shi M, Lin X-D, Chen X, Tian J-H, Chen L-J, Li K, Wang W, Eden J-S, Shen J-J, Liu L, Holmes EC, Zhang Y-Z (2018) The evolutionary history of vertebrate RNA viruses. *Nature*, 556(7700):197–202. https://doi.org/10.1038/s41586-018-0012-7

26. Moniruzzaman M, Wurch LL, Alexander H, Dyhrman ST, Gobler CJ, Wilhelm SW (2017) Virus-host relationships of marine single-celled eukaryotes resolved from metatranscriptomics. *Nature Communications*, 8(1):16054. https://doi.org/10.1038/ncomms16054

27. Urayama S, Fukudome A, Hirai M, Okumura T, Nishimura Y, Takaki Y, Kurosawa N, Koonin EV, Krupovic M, Nunoura T (2024) Double-stranded RNA sequencing reveals distinct riboviruses associated with thermoacidophilic bacteria from hot springs in Japan. *Nature Microbiology*, 9(2):514–523. https://doi.org/10.1038/s41564-023-01579-5

28. Starr EP, Nuccio EE, Pett-Ridge J, Banfield JF, Firestone MK (2019) Metatranscriptomic reconstruction reveals RNA viruses with the potential to shape carbon cycling in soil. *Proceedings of the National Academy of Sciences*, 116(51):25900–25908. https://doi.org/10.1073/pnas.1908291116

29. Callanan J, Stockdale SR, Shkoporov A, Draper LA, Ross RP, Hill C (2020) Expansion of known ssRNA phage genomes: From tens to over a thousand. *Science Advances*, 6(6):eaay5981. https://doi.org/10.1126/sciadv.aay5981

30. Urayama S, Takaki Y, Nishi S, Yoshida-Takashima Y, Deguchi S, Takai K, Nunoura T (2018) Unveiling the RNA virosphere associated with marine microorganisms. *Molecular Ecology Resources*, 18(6):1444–1455. https://doi.org/10.1111/1755-0998.12936

31. Neri U, Wolf YI, Roux S, Camargo AP, Lee B, Kazlauskas D, Chen IM, Ivanova N, Zeigler Allen L, Paez-Espino D, Bryant DA, Bhaya D, Krupovic M, Dolja VV, Kyrpides NC, Koonin EV, Gophna U, Narrowe AB, Probst AJ, Sczyrba A, Kohler A, Séguin A, Shade A, Campbell BJ, Lindahl BD, Reese BK, Roque BM, DeRito C, Averill C, Cullen D, Beck DAC, Walsh DA, Ward DM, Wu D, Eloe-Fadrosh E, Brodie EL, Young EB, Lilleskov EA, Castillo FJ, Martin FM, LeCleir GR, Attwood GT, Cadillo-Quiroz H, Simon HM, Hewson I, Grigoriev IV, Tiedje JM, Jansson JK, Lee J, VanderGheynst JS, Dangl J, Bowman JS, Blanchard JL, Bowen JL, Xu J, Banfield JF, Deming JW, Kostka JE, Gladden JM, Rapp JZ, Sharpe J, McMahon KD, Treseder KK, Bidle KD, Wrighton KC, Thamatrakoln K, Nusslein K, Meredith LK, Ramirez L, Buee M, Huntemann M, Kalyuzhnaya MG, Waldrop MP, Sullivan MB, Schrenk MO, Hess M, Vega MA, O'Malley MA, Medina M, Gilbert NE, Delherbe N, Mason OU, Dijkstra P, Chuckran PF, Baldrian P, Constant P, Stepanauskas R, Daly RA, Lamendella R, Gruninger RJ, McKay RM, Hylander S, Lebeis SL, Esser SP, Acinas SG, Wilhelm SS, Singer SW, Tringe SS, Woyke T, Reddy TBK, Bell TH, Mock T, McAllister T, Thiel V, Denef VJ, Liu W-T, Martens-Habbena W, Allen Liu X-J, Cooper ZS, Wang Z (2022) Expansion of the global RNA virome reveals diverse clades of

bacteriophages. *Cell*, 185(21):4023-4037.e18. https://doi.org/10.1016/j.cell.2022.08.023

32. Papke E, Kennedy GE, Elliott E, Taylor A, Tolar BB, Ushijima B (2024) Transmission Electron Microscopy of Coral Tissue. *Current Protocols*, 4(11):e70033. https://doi.org/10.1002/cpz1.70033

33. Hawthorn AC, Dennis M, Kiryu Y, Landsberg J, Peters E, Work TM (2024) Stony coral tissue loss disease (SCTLD) case definition for wildlife.

34. Price KL, Peters EC (2018) Histological Techniques for Corals.

35. Luna LG (1968) Manual of histologic staining methods of the Armed Forces Institute of Pathology. *Manual of histologic staining methods of the Armed Forces Institute of Pathology*, :xii, 258–xii, 258.

36. Quintero-Hunter I, Grier H, Muscato M (1991) Enhancement of histological detail using metanil yellow as counterstain in periodic acid Schiff's hematoxylin staining of glycol methacrylate tissue sections. *Biotechnic & Histochemistry*, 66(4):169–172.

37. Schneider CA, Rasband WS, Eliceiri KW (2012) NIH Image to ImageJ: 25 years of image analysis. *Nature Methods*, 9(7):671–675. https://doi.org/10.1038/nmeth.2089

38. Landsberg JH (2020) Stony Coral Tissue Loss Disease in Florida Is Associated With Disruption of Host–Zooxanthellae Physiology. *Frontiers in Marine Science*, 7:24.

39. Grottoli AG, Toonen RJ, Van Woesik R, Vega Thurber R, Warner ME, McLachlan RH, Price JT, Bahr KD, Baums IB, Castillo KD, Coffroth MA, Cunning R, Dobson KL, Donahue MJ, Hench JL, Iglesias-Prieto R, Kemp DW, Kenkel CD, Kline DI, Kuffner IB, Matthews JL, Mayfield AB, Padilla-Gamiño JL, Palumbi S, Voolstra CR, Weis VM, Wu HC (2021) Increasing comparability among coral bleaching experiments. *Ecological Applications*, 31(4):e02262. https://doi.org/10.1002/eap.2262